The Astrophysical Journal, 650:350–373, 2006 October 10


# SILICON AND CARBON ISOTOPIC RATIOS IN AGB STARS: SiC GRAIN DATA, MODELS, AND THE GALACTIC EVOLUTION OF THE Si ISOTOPES

Ernst Zinner,[1] Larry R. Nittler,[2] Roberto Gallino,[3,4] Amanda I. Karakas,[5]
Maria Lugaro,[6] Oscar Straniero,[7] and John C. Lattanzio[4]

*Received 2005 December 16; accepted 2006 May 29*

## ABSTRACT

Presolar SiC grains of the mainstream, Y, and Z type are believed to come from carbon stars. We compared their C and Si isotopic ratios with theoretical models for the envelope compositions of AGB stars. Two sets of models (FRANEC and Monash) use a range of stellar masses (1.5–5 $M_{\odot}$) and metallicities, different prescriptions for mass loss, and two sets of neutron-capture cross sections for the Si isotopes. They predict that the shifts in Si isotopic ratios and the increase of $^{12}C/^{13}C$ in the envelope during third dredge-up are higher for higher stellar mass, lower metallicity, and lower mass-loss rate. Because the $^{22}Ne$ neutron source dominates Si nucleosynthesis, the effect of the $^{13}C$ source is negligible. Comparison of the model predictions with grain data confirms an AGB origin for these grains, with Y and Z grains having originated in stars with lower than solar metallicity. The Si isotopic ratios of the Z grains favor the Si cross sections by Guber et al. over those by Bao et al. The $^{12}C/^{13}C$ ratios of low-metallicity models are much higher than those found in Z grains, and cool bottom processing must be invoked to explain the grains' C isotopic ratios. By combining Z grain Si data with the models, we determined the evolution of the $^{29}Si/^{28}Si$ ratio in the Galaxy as function of metallicity $Z$. At $Z < 0.01$ this ratio rises much faster than current Galactic evolution models predict and suggests an early source of the heavy Si isotopes not considered in these models.

*Subject headings:* dust, extinction — Galaxy: evolution — nuclear reactions, nucleosynthesis, abundances — stars: AGB and post-AGB — stars: carbon

## 1. INTRODUCTION

Primitive meteorites contain presolar grains, grains that formed before the Sun in the atmospheres of late-type stars and in supernova (SN) ejecta. They are thus stardust that survived interstellar travel, the formation of the solar system, and processes on the parent bodies of the meteorites in which they are found today. After extraction from meteorites they can be studied in detail in the laboratory (Bernatowicz & Zinner 1997; Zinner 1998, 2003; Hoppe & Zinner 2000; Nittler 2003; Clayton & Nittler 2004). Their stellar origins are indicated by their isotopic compositions that are completely different from those found in solar system materials (e.g., Zinner 1998). The isotopic compositions of the grains thus provide information about specific stages in the evolution of their parent stars.

Presolar grain types identified so far include diamonds (Lewis et al. 1987), silicon carbide (SiC; Bernatowicz et al. 1987; Tang & Anders 1988), graphite (Amari et al. 1990), refractory carbides such as TiC (Bernatowicz et al. 1991, 1996), oxides (corundum, $Al_2O_3$; spinel, $MgAl_2O_4$; and hibonite, $CaAl_{12}O_{19}$; Huss et al. 1994; Hutcheon et al. 1994; Nittler et al. 1994, 1997; Choi et al. 1999), silicon nitride ($Si_3N_4$; Nittler et al. 1995), and various silicates (e.g., olivine, pyroxene, and nonstoichiometric phases; Messenger et al. 2003; Nguyen & Zinner 2004; Mostefaoui & Hoppe 2004; Nagashima et al. 2004). Transmission electron microscopy (TEM) studies of presolar graphite grains also revealed subgrains of refractory carbides such as titanium carbide (TiC) and cohenite [$(Fe,Ni)_3C$] as well as kamacite (Fe-Ni metal) and elemental Fe (Bernatowicz et al. 1991, 1996; Croat et al. 2003, 2005).

Of all the presolar grains, SiC, the third most abundant grain type, with concentrations in primitive meteorites ranging up to ~30 ppm (parts per million; Amari et al. 1994; Huss & Lewis 1995; Newton et al. 1995), has been studied in greatest detail. The reason is that SiC is relatively rich in trace elements (Amari et al. 1995a) and grains can be as large as several $\mu$m, which makes it possible to measure isotopic ratios of many elements by secondary ion mass spectrometry (SIMS) in the ion microprobe (Zinner 1998) and/or by resonance ionization mass spectrometry (RIMS; Nicolussi et al. 1997, 1998b; Lugaro et al. 2003a; Savina et al. 2004).

Based on C, N, and Si isotopic ratios measured in single grains (Figs. 1 and 2), SiC has been classified into different types (Hoppe et al. 1994; Hoppe & Ott 1997). Most grains (~93%), defined as "mainstream" grains, have isotopically heavy C ($^{12}C/^{13}C = 20$–100; solar = 89) and light N ($^{14}N/^{15}N > 272$ = terrestrial). In Figure 1 we take the terrestrial N isotopic ratios of 272 to be solar. The solar ratio is unknown but might be better represented by the ratio measured in Jupiter, which is ~430 (Owen et al. 2001). Silicon is usually enriched in the neutron-rich isotopes, by up to 200‰ (parts per thousand). Analyses of SiC bulk samples (≡ aggregates of many grains), which are dominated by mainstream grains, have shown strong *s*-process signatures for the noble gases Kr and Xe as well as the heavy elements Sr, Ba, Nd, and Sm (see Hoppe & Ott 1997; Gallino et al. 1997). Recently, RIMS measurements of heavy-element isotopic ratios have revealed *s*-process Sr, Zr, Mo, Ru, and Ba (Nicolussi et al. 1997, 1998a; Lugaro et al.

[1] Laboratory for Space Sciences and Physics Department, Washington University, One Brookings Drive, St. Louis, MO 63130; ekz@wustl.edu.
[2] Department of Terrestrial Magnetism, Carnegie Institution of Washington, 5241 Broad Branch Road NW, Washington, DC 20015.
[3] Dipartimento di Fisica Generale, Università di Torino, Via P. Giuria 1, I-10125 Torino, Italy.
[4] Centre for Stellar and Planetary Astrophysics, School of Mathematical Sciences, Monash University, Clayton, VIC 3800, Australia.
[5] Department of Physics and Astronomy, McMaster University, 1280 Main Street W, Hamilton, ON L8S 4M1, Canada.
[6] Astronomical Institute, University of Utrecht, Postbus 80000, 3508 TA Utrecht, Netherlands.
[7] INAF–Osservatorio Astronomico di Teramo, Via M. Maggini 47, 64100 Teramo, Italy.

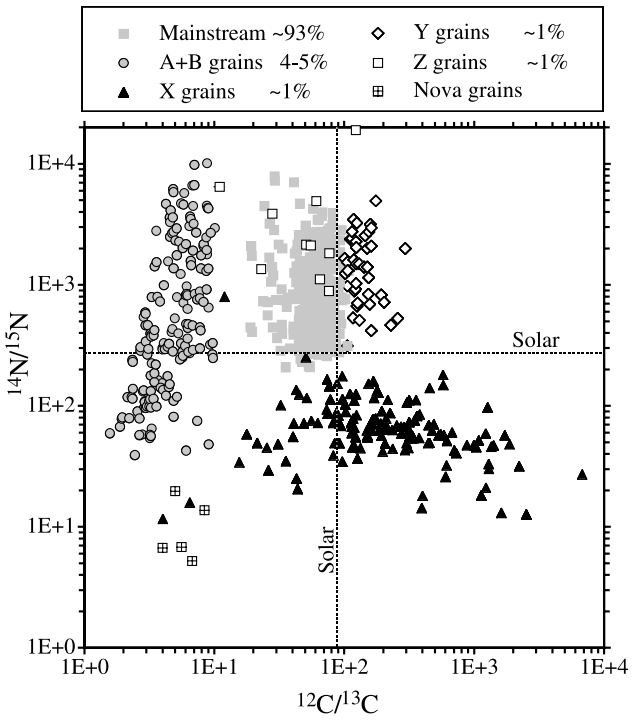


FIG. 1.—Nitrogen and C isotopic ratios of individual presolar SiC grains. Because rare grain types were located by automatic ion imaging, the numbers of grains of different types plotted in the figure do not correspond to their abundances in the meteorites; these abundances are given in the legend. Data are from Alexander (1993), Hoppe et al. (1994, 1996a), Nittler et al. (1995), Huss et al. (1997), and Amari et al. (2001a, 2001b, 2001c).

2003a; Savina et al. 2004) in individual mainstream SiC grains. Thermally pulsing asymptotic giant branch (TP-AGB) stars are believed to be the source of the main *s*-process component in the solar system elemental abundance distribution. They also provide a C-rich environment, where SiC grains can form. Such stars are therefore the most likely stellar sources of the mainstream grains (e.g., Gallino et al. 1997; Lugaro et al. 2003a). The isotopic ratios of the light elements C and N also point to an AGB star origin (Gallino et al. 1994; Hoppe et al. 1994; Lugaro et al. 1999).

Silicon carbide grains of type X (~1% of total SiC) have isotopically light C and heavy N, as well as high inferred $^{26}Al/^{27}Al$ ratios (~0.1, up to 0.6) and large $^{28}Si$ excesses (Nittler et al. 1995; Hoppe et al. 2000). These isotopic signatures, but most conclusively large $^{44}Ca$ excesses from the decay of $^{44}Ti$ ($T_{1/2} = 60$ yr; Nittler et al. 1996; Hoppe et al. 1996b) and large $^{49}Ti$ excesses from the decay of $^{49}V$ ($T_{1/2} = 337$ days; Hoppe & Besmehn 2002), show that these grains must have originated from supernovae. Grains of type A and B (~3%–4% of presolar SiC) have $^{12}C/^{13}C$ ratios of less than 10, but the distribution of their Si isotopic ratios is similar to that of the mainstream grains. J-type carbon stars and post-AGB stars that undergo a very late thermal pulse (e.g., Sakurai's object; Asplund et al. 1999) have been proposed as sources of A + B grains (Amari et al. 2001c), but the details of the nucleosynthetic processes that would produce the isotopic signatures of these grains are still not well understood. A few SiC grains have low $^{12}C/^{13}C$ and $^{14}N/^{15}N$, high inferred initial $^{26}Al/^{27}Al$, and large $^{30}Si$ excesses, relative to solar system ratios, indicative of an origin in nova ejecta (Amari et al. 2001a), although a SN origin is possible for these grains as well (Nittler & Hoppe 2005).

Grains of type Y (~1% of total SiC) are defined as having $^{12}C/^{13}C$ ratios larger than 100 and being enriched in $^{30}Si$ compared with mainstream grains (Amari et al. 2001b; see Figs. 1 and 2), while Z grains (~1% of total SiC; Hoppe et al. 1997a) show a range of $^{12}C/^{13}C$ ratios similar to that of mainstream grains, but typically have $^{29}Si$ depletions and even larger $^{30}Si$ excesses than Y grains. Amari et al. (2001b) proposed that Y grains formed in AGB stars of approximately half solar metallicity ($Z = 0.01$ or $[Fe/H] = -0.3$, using the spectroscopic notation $[Fe/H] = \log(Fe/H) - \log(Fe/H)_{\odot}$) with masses ranging from 1.5 to possibly $5M_{\odot}$, while Hoppe et al. (1997a) suggested that Z grains formed in low-mass ($M < 2.3\ M_{\odot}$), low-metallicity ($Z = 0.006$ or $[Fe/H] = -0.52$) AGB stars that had experienced extra mixing in addition to the third dredge-up (Charbonnel 1995; Wasserburg et al. 1995; Nollett et al. 2003).

While SNe are the source of X grains, novae are possibly the parent stars of a few SiC grains, and J stars and post-AGB stars have been proposed as the sources of A + B grains, all available evidence points to low-mass (1–3 $M_{\odot}$) AGB stars during their TP phase as sources of the mainstream, Y, and Z grains. Such stars undergo substantial mass loss by stellar winds, finally losing their entire envelope, while the degenerate C-O core is left behind as a nascent white dwarf. During the TP phase the envelope of such stars is progressively enriched in carbon ($^{12}C$) and in *s*-process elements by recurrent mixing of material from shell-burning zones in the third dredge-up (TDU). Eventually, the stellar envelope may become C-rich (and the star an N-type carbon star), a necessary condition for the condensation of SiC grains in the stellar outflow.

The isotopic compositions of the elements C, N, and Ne and the heavy elements (Sr and heavier) in SiC grains that originated from carbon stars are dominated by nucleosynthetic processes in the parent stars of the grains. For C, N, and Ne these processes are H burning via the CNO cycle during the main-sequence phase of the star followed by the first (and second) dredge-up (El Eid 1994) and shell He burning and the TDU during the TP-AGB phase (Busso et al. 1999). For low-mass stars, deep mixing of envelope material ("cool bottom processing"; Wasserburg et al. 1995; Nollett et al. 2003) to hot regions has been invoked to explain the low $^{12}C/^{13}C$ ratios in carbon stars (Charbonnel 1995; Abia & Isern 1997; Boothroyd & Sackmann 1999) and apparently also plays an important role for the grains. The heavy elements are affected by the *s*-process, neutron capture at low neutron densities (Gallino et al. 1997; Hoppe & Ott 1997; Busso et al. 1999; Lugaro et al. 2003a).

While the isotopic compositions of Si (and Ti) are also affected by neutron capture, predicted changes of the isotopic ratios of these elements in a single star cannot account for the range of isotopic ratios observed in mainstream SiC grains (Lugaro et al. 1999). This observation led to the proposal that several stars with a range of initial isotopic ratios contributed SiC grains to the solar system (Clayton et al. 1991; Alexander 1993). In this view the Si (and Ti) isotopic compositions of mainstream (and type Y and Z) SiC grains reflect both the initial isotopic compositions of the parent stars and the effect of neutron capture in the TP-AGB parent stars of the grains. Several explanations have been advanced for the Si isotopic compositions of the parent stars. One is the evolution of the Si isotopic ratios through Galactic history (the Galactic chemical evolution, GCE). Early generations of Type II supernovae (SNe II) produced mainly $^{28}Si$. As the metallicity of the Galaxy increased, later generations of stars produced increasing amounts of $^{29}Si$ and $^{30}Si$, so that throughout Galactic history the $^{29}Si/^{28}Si$ and $^{30}Si/^{28}Si$ ratios continuously increased (Timmes & Clayton 1996; Clayton & Timmes 1997; Alexander & Nittler

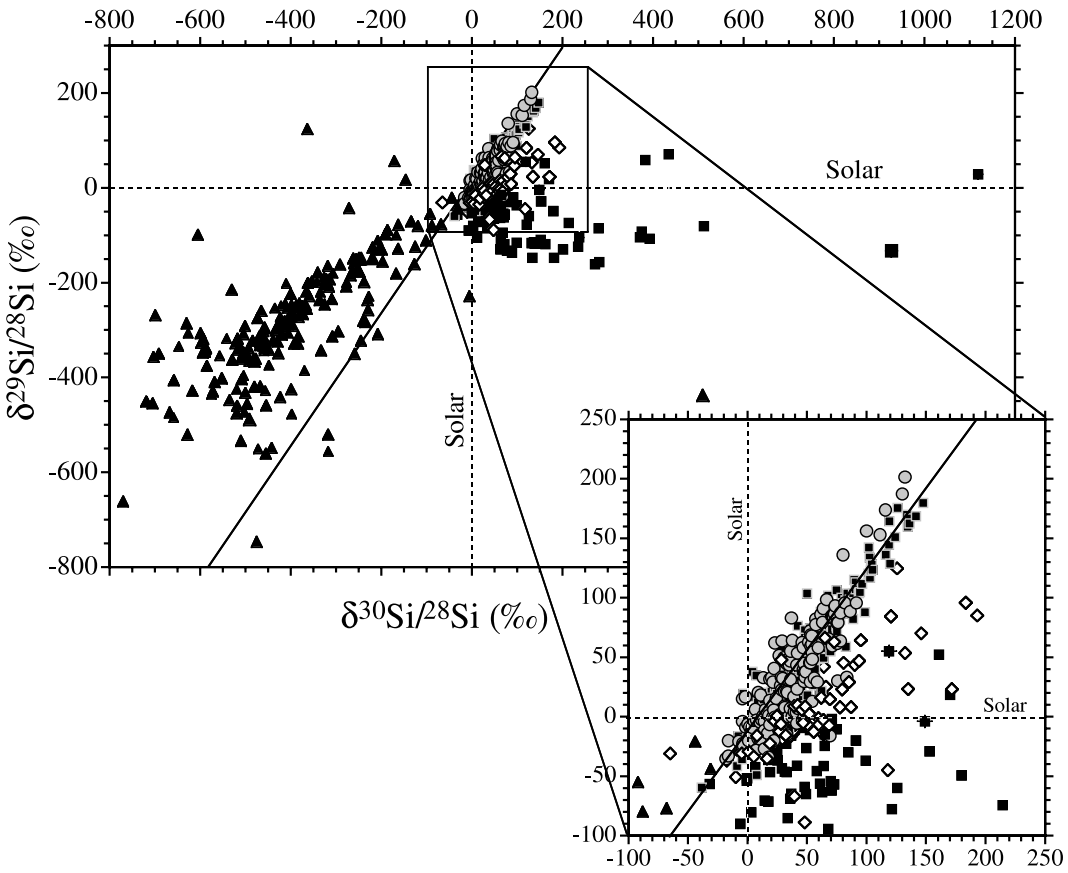


FIG. 2.—Silicon isotopic ratios of different types of presolar SiC grains plotted as $\delta$-values, deviations in permil (‰) from the solar ratios: $\delta^i\mathrm{Si}/^{28}\mathrm{Si} = [(\delta^i\mathrm{Si}/^{28}\mathrm{Si})_{\mathrm{meas}}/(\delta^i\mathrm{Si}/^{28}\mathrm{Si})_{\odot} - 1] \times 1000$. Mainstream grains plot along a line of slope 1.35 (*solid line*). Symbols are the same as those in Fig. 1. Data are from the same sources as for Fig. 1.

1999). A second explanation was given by Lugaro et al. (1999), who proposed that the spread in the Si isotopic ratios of the parent stars was caused by local heterogeneities in the Galaxy that reflected the stochastic nature of the admixture of the ejecta from supernovae of different types and masses. Both processes must have contributed to the distribution of the Si isotopic ratios in the SiC parent stars, although Nittler (2005) argued that the observed correlation between Si and Ti isotopes in SiC grains indicates a minor role for local heterogeneities. A third explanation was given by Clayton (2003), who postulated that a merger of a low-metallicity satellite galaxy with the Milky Way was responsible for the range of Si isotopic ratios inferred for the parent stars of mainstream SiC grains.

Figure 3 demonstrates schematically three processes that are responsible for the Si isotopic compositions of presolar SiC grains from carbon stars in a Si three-isotope plot. The Si isotopic ratios are plotted as $\delta$-values, deviations from the solar ratios in permil (‰). The Galactic evolution leads to a continuous increase of the $^{29}\mathrm{Si}/^{28}\mathrm{Si}$ and $^{30}\mathrm{Si}/^{28}\mathrm{Si}$ ratios as a function of time. The exact evolutionary path in the three-isotope plot is not known. We assume that it is a straight line from pure $^{28}\mathrm{Si}$ ($\delta^{29}\mathrm{Si}/^{28}\mathrm{Si} = \delta^{30}\mathrm{Si}/^{28}\mathrm{Si} = -1000$‰) through the solar composition point ($\delta^{29}\mathrm{Si}/^{28}\mathrm{Si} = \delta^{30}\mathrm{Si}/^{28}\mathrm{Si} = 0$). This assumes that the solar isotopic ratios are representative for the local Galactic ratios at the time of solar system formation, or more generally that the Sun is representative of stars at $[\mathrm{Fe/H}] = 0$, a point that has been variously discussed (Clayton 1997; Alexander & Nittler 1999). At any given time there probably was and is a variety of isotopic ratios in the Galaxy. First,

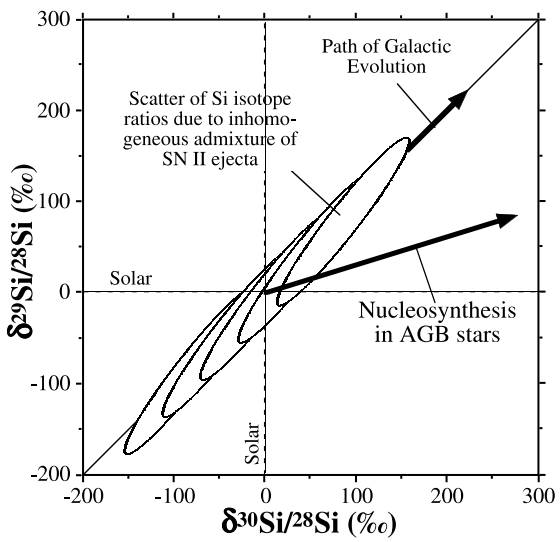


FIG. 3.—Schematic representation of processes that affect the Si isotopic compositions of presolar SiC grains with an origin in C-rich AGB stars. The Galactic evolution of the Si isotopes, assumed to progress along a slope 1 line, is broadened due to heterogeneous admixture of the ejecta of supernovae. Neutron capture in AGB stars shifts the original Si isotopic ratios of the grain's parent stars to the right of the Galactic evolution line.

there exist systematic differences as function of Galactic radius because of the radial gradient of metallicity in the Galaxy (Clayton 1997). But even locally there must have been heterogeneities in the elemental and isotopic ratios (Edvardsson et al. 1993; Nordström et al. 2004; Andersen et al. 2005). For Si this is schematically indicated by a series of ellipses, each of which represents the local heterogeneity at a given Galactic time. As a function of time these ellipses move along the path of overall Galactic evolution of the Si isotopes. In the Galactic merger model by Clayton (2003), not shown in the figure, the range of Si isotopic ratios in the parent stars is explained as a mixing line between a low-metallicity component with low Si isotopic ratios (satellite galaxy) and a high-metallicity component with high Si isotopic ratios (Milky Way) along the Galactic evolution path in the figure. Neutron capture during the TP-AGB phase and TDU is expected to result in envelope compositions that are shifted to the right of the Galactic evolutionary path.

Both the Galactic component (involving GCE and local heterogeneity) and the nucleosynthetic component of the Si isotopic ratios of SiC grains depend on the metallicity of the parent stars. A low-metallicity star is expected to have initial $^{29}Si/^{28}Si$ and $^{30}Si/^{28}Si$ ratios that are smaller than the solar ratios. The isotopic shifts due to neutron capture depend on both metallicity and stellar mass. The shifts are larger for smaller metallicity and for larger mass. Amari et al. (2001b) and Zinner et al. (2001) have compared the Si isotopic ratios of mainstream, Y, and Z SiC grains with theoretical predictions for the modifications of the Si isotopes by neutron capture in AGB stars of different masses and metallicities (Lugaro et al. 1999) and used general concepts of GCE to derive the evolution of the Si isotopic ratios as a function of metallicity in the Galaxy. In this paper we are taking up this investigation again. This is prompted by three developments during the last few years. First, recent isotopic measurements of large numbers of presolar SiC grains (Nittler & Alexander 2003; Zinner et al. 2003, 2005, Nittler & Hoppe 2005) have vastly increased the grain database beyond that used by Amari et al. (2001b) and Zinner et al. (2001), especially for the rare Z grains. Second, new stellar evolution models of low- to medium-mass stars through the AGB phase have become available (Karakas 2003; Straniero et al. 2003, 2006; Karakas et al. 2006), encompassing a larger range of masses and metallicities. Finally, Guber et al. (2003) reported new measurements of the neutron-capture cross sections affecting the Si isotopes, indicating significant changes relative to the values (Bao et al. 2000) adopted by Lugaro et al. (1999) for their theoretical predictions of Si isotopic abundances in the envelopes of AGB stars during TDU.

In this paper we compare the C and Si isotopic compositions of mainstream, Y, and Z grains with theoretical predictions of new stellar evolution models for AGB stars of different metallicities, masses, and different prescriptions and rates for the mass loss in an attempt to understand the Galactic evolution of the Si isotopic ratios. After a discussion of the grain database (§ 2), we present in § 3 two sets of stellar evolution models with post-processing codes and give the predicted changes in the C and Si isotopic ratios in the AGB star envelope. In § 4 we compare the theoretical predictions with grain data to determine the most likely parent stars of the grains. Section 5, where we use a set of model predictions and the grain data to determine the Galactic evolutions of the Si isotopic ratios, is followed by some conclusions (§ 6).

It would be highly desirable to make this same comparison also for the Ti isotopic ratios of the grains. However, the number of precise Ti isotopic ratio measurements of SiC grains is still limited. The advent of a new ion microprobe, the Cameca NanoSIMS, and the high spatial resolution and sensitivity of this instrument (Slodzian et al. 2003; Amari et al. 2003) give us hope that this will be achieved in the near future.

## 2. SiC GRAINS AND THEIR C AND Si ISOTOPIC COMPOSITIONS

Since the first isotopic measurements on presolar SiC grains (Zinner et al. 1987), a large number of measurements have been made on individual grains, and today the number of analyzed grains exceeds 7000. However, in spite of these efforts we do not have the C and Si isotopic compositions of an unbiased sample of SiC grains. There are several reasons for this. First, presolar SiC grains have a large range of sizes, from 100 nm to 20 $\mu$m (Amari et al. 1994), but because of instrumental limitations, isotopic analyses were until recently mostly restricted to the larger grains in this distribution. Second, size distributions vary among different meteorites (Huss et al. 1997; Russell et al. 1997), and as a consequence the size distribution of presolar SiC in the solar system is not well defined. Because of availability and because SiC grains from the Murchison carbonaceous chondrite are, on average, larger than those from other meteorites, most analyzed grains have been from Murchison. Another reason is that special searches were made for rare grain types in direct imaging mode (Nittler 1996), and candidate grains were subsequently analyzed individually for their isotopic compositions. These searches were made using different isotopic ratios and different conditions. The $^{30}Si/^{28}Si$ ratio measured at low mass resolution was used to search for presolar SiC grains of type X, characterized by $^{28}Si$ excesses (Nittler et al. 1995; Hoppe et al. 1996b, 2000; Lin et al. 2002; Besmehn & Hoppe 2003). At low mass resolution the interference from $^{29}SiH$ at mass 30 is negligible. This search also yields candidates for Z grains with large $^{30}Si$ excesses, but Z grains with only moderate $^{30}Si$ excesses are missed, because $^{29}Si$ is not measured. Searches for A + B grains were made by imaging of the C isotopic ratios at low mass resolution (Amari et al. 2001c), but the search for Y grains required the use of high mass resolution imaging because of the interference from $^{12}CH$ at mass 13 for the high $^{12}C/^{13}C$ ratios characterizing these grains (Amari et al. 2001b).

Two new developments have helped in identifying SiC grains of type Y and type Z. One was an automated isotopic measurement system for the Cameca ims 6f ion microprobe by Nittler & Alexander (2003) that allows C and Si isotopic analysis of individual SiC grains at high mass resolution. These authors analyzed ~3300 presolar SiC grains from Murchison in the size range 0.5–4 $\mu$m in this way. In this sample they found the abundances of Y and Z grains to be 1.5% and 1.4%, respectively. A second development was the arrival of a new type of ion microprobe, the NanoSIMS (Slodzian et al. 2003, 2004). This instrument, with its high spatial resolution and high sensitivity, makes the isotopic analysis of small presolar grains possible. One advantage for locating Y and Z grains is that the abundance of these grain types among all presolar SiC grains increases with decreasing grain size (Hoppe et al. 1996a, 1997b). Amari and Zinner and coworkers (Amari et al. 2002; Zinner et al. 2003, 2005) analyzed submicron individual SiC grains and found the abundance of Y grains among 310 SiC grains from the Murchison separate KJB (average grain size 0.49 $\mu$m) to be 6.5% and the abundances of Y and Z grains among SiC grains from the Indarch enstatite (EH3) chondrite (average grain size 0.4 $\mu$m) to be 5.9% (of 696 grains) and 7.6% (of 542 grains), respectively.

For all these reasons the C and Si data of mainstream, Y, and Z SiC grains used in this paper cannot be considered to reflect a representative sample of presolar SiC grains in the solar system. However, we deem this to be only a minor defect, because we

consider mostly the range of isotopic compositions for these different grain types and pay only minor attention to the detailed distribution and abundance within these ranges. Our database includes the measurements reported by Alexander (1993), Hoppe et al. (1994, 1996a, 1997b), Huss et al. (1997), Amari et al. (2001b), Nittler & Alexander (2003), Zinner et al. (2003, 2005), and Nittler & Hoppe (2005). In these data we eliminated grains with errors >15‰ for the Si isotopic ratios. The criteria for distinguishing between grain types used by different authors (Hoppe & Ott 1997; Zinner 1998; Nittler & Alexander 2003) are not entirely consistent with one another. One reason probably is that in the early days only few examples of rare grain types were known. Another reason for possible ambiguity is that although the different SiC types are fairly well separated in their C, N, and Si isotopic distributions (Figs. 1 and 2), there are some regions of overlap. We define as mainstream grains those with $10 < {}^{12}C/{}^{13}C < 100$, excluding X grains (having $^{15}N$ and $^{28}Si$ excesses) and Z grains (see below); as Y grains those with $^{12}C/^{13}C > 100$ and $^{14}N$ excesses; and as Z grains those with $10 < {}^{12}C/{}^{13}C < 100$ and either $\delta^{29}Si < 0$ and lying to the $^{30}Si$-rich side of the mainstream correlation line, or $\delta^{29}Si > 0$ and lying to the right of the mainstream line by more than 50‰.

## 3. MODELS FOR THE NUCLEOSYNTHESIS OF C AND Si ISOTOPES IN AGB STARS

In order to compare the C and Si isotopic ratios in mainstream, Y, and Z grains we computed the evolution of the C and Si isotopic ratios in the envelopes of AGB stars for a large set of stellar models. Two different sets of models were produced. One was produced at the University of Torino, based on the FRANEC stellar evolution models, and the other at Monash University. The two sets of models differ in various detailed assumptions, such as mass loss, and we wanted to determine to what degree the predicted isotopic ratios depend on these assumptions. Both sets of models consist of a stellar evolution code, which uses only certain nuclear reactions important for energy production and computes the stellar structure through the AGB phase, and a postprocessing code that takes the results of the structure code as input parameters and computes nuclear reactions occurring during the TP-AGB phase for an extended network of many elements and isotopes.

During the AGB phase H and He burn alternately in shells situated above the degenerate C-O core. Between the H- and the He-burning shells is located a thin region (He intershell) whose mass is of the order of $\sim 10^{-2}\ M_\odot$ in stellar models of mass $\leq 4\ M_\odot$ and of $\sim 10^{-3}\ M_\odot$ in stellar models of higher mass (Straniero et al. 1997, 2000). When He burning sets in, a thermal runaway occurs, driving the formation of a convective zone (thermal pulse, or TP) in the He intershell for a short period of time, on the order of 100 yr in models of mass $\lesssim 4\ M_\odot$ and of 10 yr in models of higher mass. This thermal pulse results in the expansion and cooling of the overlying regions so that the H shell becomes temporarily inactive. Soon after the quenching of the TP and before the H-burning shell becomes active again, the base of the convective envelope moves inward and can penetrate into the top layers of the He intershell. By this process freshly synthesized material is mixed into the envelope and appears at the stellar surface (third dredge-up episode, TDU). The He intershell is rich in $^{12}C$, produced by partial He burning during the convective thermal pulse, and in heavy elements such as Sr and Ba, produced by the *s*-process (Busso et al. 1999). After a number of TDU episodes, the C/O ratio in the stellar envelope may become larger than unity, resulting in a carbon star. This is a necessary condition for the formation of SiC grains. The isotopic compositions of intermediate-mass elements, such as Si, are slightly modified by neutron-capture nucleosynthesis in the He intershell. In summary, during the TP-AGB phase, because of the combined effect of neutron captures in the He intershell and the occurrence of the TDU, the Si isotopic ratios are modified at the stellar surface.

Neutron captures in the He intershell of AGB stars are driven by the activation of two neutron source reactions: $^{13}C(\alpha, n)^{16}O$ and $^{22}Ne(\alpha, n)^{25}Mg$. The first of these reactions occurs under radiative conditions during the interval between thermal pulses (Straniero et al. 1997) and is responsible for the production of the bulk of heavy elements via the *s*-process (Gallino et al. 1998; Goriely & Mowlavi 2000; Lugaro et al. 2003b). The formation of a region rich in $^{13}C$ ($^{13}C$ pocket) in the He intershell is related to phenomena whose nature is still a matter of debate, and there are large uncertainties associated with the detailed features of the $^{13}C$ pocket (Busso et al. 1999; Denissenkov & Tout 2003; Herwig et al. 2003; Lugaro et al. 2003b). Current models assume that a $^{13}C$ pocket of mass $\sim 10^{-3}\ M_\odot$ ($\sim$10% of the intershell mass in 3 $M_\odot$ stars) forms immediately below the H/He discontinuity left behind by the TDU. This pocket contains $3.1 \times 10^{-6}\ M_\odot$ of $^{13}C$ distributed over a zone with decreasing $^{13}C$ abundance as a function of depth ("standard case"; Gallino et al. 1998). As has previously been shown by Lugaro et al. (1999), the Si isotopic composition is mostly affected by the neutron flux produced by the $^{22}Ne$ source, and the Si isotopic ratios do not change significantly when the amount of $^{13}C$ in the He intershell is varied by factors from 0.08 to 2 relative to the "standard" amount chosen by Gallino et al. (1998). This behavior is essentially due to the low neutron-capture cross sections of Si isotopes and to the fact that the $^{13}C$ pocket has a small mass compared to the mass of the He intershell. When the next convective TP develops, the $^{13}C$ pocket material is distributed over the whole He intershell and is diluted typically by a factor of 10 in mass. A fraction of the material engulfed by the TP is composed of material that had been processed by the previous TP, the overlap factor between subsequent pulses being roughly 1/2 for stars of masses $\lesssim 3\ M_\odot$. The remaining material in the TP is composed of H-burning ashes, where Si isotopes are present in the original proportions. The Si isotopic ratios in the TP are barely changed by the small addition of Si modified in its isotopic composition by the $^{13}C$ neutron source. The Si isotopic ratios are instead affected by the activation of the $^{22}Ne$ neutron source. In a TP a large amount of $^{22}Ne$ is produced during the early development of the convective instability by double $\alpha$-captures on abundant $^{14}N$ left in the H-burning ashes. The activation of the $^{22}Ne$ neutron source in the thermal pulse is sensitive to the maximum temperature reached at the base of the convective region, which increases with increasing mass and decreasing metallicity of the star. In summary, the final Si isotopic ratios in the envelope are insensitive, for a given stellar model, to the choice of the features of the $^{13}C$ pocket. However, they depend for different stellar models on the temperature at the base of the TPs, the amount of TDU, and the adopted mass-loss rate.

### 3.1. *Torino Models*

To model the nucleosynthesis in the He intershell we have made use of a postprocessing code that computes neutron captures on nuclei from C to Po (Gallino et al. 1998). The evolution of the nuclear abundances at the stellar surface is obtained by mixing He intershell material by TDU into a mass-losing envelope. Stellar structure features such as the envelope mass, the dredged-up mass, the temperature and density at the base of the convective pulse, and their dependence on time and mass during the convective TP are needed as input for the postprocessing code.

TABLE 1

PARAMETERS OF DIFFERENT STELLAR EVOLUTION MODELS OBTAINED FROM THE FRANEC CODE AND FROM AN ANALYTICAL FORMULA DERIVED FROM THIS CODE

| Mass | $Z$ | $\eta$ | TDU Episodes | TDU Mass ($M_\odot$) | TDU with C/O > 1 | Final $M_{env}$ | Final C/O | $^{12}C/^{13}C$ at C/O = 1 | Final $^{12}C/^{13}C$ | $\delta^{29}Si$ at C/O = 1 Bao | Final $\delta^{29}Si$ Bao | $\delta^{30}Si$ at C/O = 1 Bao | Final $\delta^{30}Si$ Bao | $\delta^{29}Si$ at C/O = 1 Guber | Final $\delta^{29}Si$ Guber | $\delta^{30}Si$ at C/O = 1 Guber | Final $\delta^{30}Si$ Guber |
|---|---|---|---|---|---|---|---|---|---|---|---|---|---|---|---|---|---|
| 1.5[a] | 0.02 | 0.1 | 24 | 0.017 | 12 | 0.56 | 1.50 | 39 | 56 | 4 | 11 | 4 | 14 | 1 | 5 | 9 | 26 |
| | | 0.3 | 19 | 0.010 | 6 | 0.34 | 1.15 | 37 | 42 | 4 | 6 | 5 | 8 | 2 | 3 | 11 | 15 |
| | | 0.5 | 9 | 0.003 | 0 | 0.28 | 0.56 | ... | ... | ... | ... | ... | ... | ... | ... | ... | ... |
| | 0.01 | 0.1 | 24 | 0.026 | 17 | 0.57 | 2.98 | 48 | 149 | −65 | −46 | −65 | −35 | −66 | −59 | −62 | −14 |
| | | 0.3 | 19 | 0.011 | 12 | 0.33 | 2.12 | 48 | 105 | −65 | −56 | −65 | −51 | −66 | −63 | −61 | −39 |
| | | 0.5 | 10 | 0.004 | 0 | 0.29 | 0.86 | ... | ... | ... | ... | ... | ... | ... | ... | ... | ... |
| | 0.006 | 0.1 | 24 | 0.044 | 20 | 0.58 | 7.08 | 60 | 458 | −112 | −74 | −112 | −41 | −113 | −97 | −111 | −20 |
| | | 0.3 | 19 | 0.024 | 15 | 0.34 | 4.96 | 60 | 313 | −112 | −89 | −112 | −69 | −113 | −103 | −110 | −55 |
| | | 0.5 | 9 | 0.007 | 6 | 0.46 | 2.04 | 60 | 124 | −113 | −108 | −113 | −105 | −113 | −112 | −111 | −101 |
| | 0.003 | 0.1 | 25 | 0.089 | 23 | 0.59 | 17.3 | 79 | 1660 | −172 | −12 | −172 | 146 | −173 | −105 | −172 | 242 |
| | | 0.3 | 20 | 0.050 | 18 | 0.36 | 12.9 | 80 | 1170 | −172 | −71 | −172 | 26 | −172 | −130 | −171 | 86 |
| | | 0.5 | 12 | 0.021 | 11 | 0.30 | 7.27 | 79 | 621 | −173 | −140 | −173 | −115 | −173 | −160 | −173 | −95 |
| 2[a] | 0.02 | 0.1 | 30 | 0.041 | 19 | 1.04 | 2.00 | 37 | 75 | 4 | 16 | 4 | 21 | 1 | 7 | 9 | 37 |
| | | 0.3 | 27 | 0.033 | 16 | 0.78 | 1.84 | 37 | 69 | 4 | 14 | 4 | 17 | 4 | 6 | 9 | 32 |
| | | 0.5 | 22 | 0.021 | 11 | 0.42 | 1.50 | 37 | 56 | 3 | 9 | 3 | 11 | 1 | 4 | 8 | 22 |
| | 0.01 | 0.1 | 30 | 0.083 | 24 | 1.06 | 4.14 | 49 | 211 | −66 | −38 | −66 | −21 | −66 | −55 | −63 | 2 |
| | | 0.3 | 27 | 0.050 | 21 | 0.81 | 3.76 | 48 | 190 | −66 | −42 | −66 | −29 | −66 | −57 | −63 | −8 |
| | | 0.5 | 25 | 0.042 | 19 | 0.65 | 3.50 | 48 | 177 | −66 | −45 | −66 | −33 | −66 | −58 | −63 | −15 |
| | 0.006 | 0.1 | 30 | 0.108 | 26 | 1.08 | 9.03 | 60 | 593 | −113 | −37 | −113 | 17 | −113 | −82 | −111 | 73 |
| | | 0.3 | 27 | 0.087 | 24 | 0.84 | 8.19 | 60 | 532 | −113 | −50 | −113 | −7 | −113 | −88 | −111 | 40 |
| | | 0.5 | 26 | 0.059 | 22 | 0.66 | 7.58 | 59 | 489 | −113 | −59 | −113 | −24 | −113 | −92 | −111 | 18 |
| | 0.003 | 0.1 | 30 | 0.213 | 28 | 1.10 | 23.6 | 79 | 2421 | −173 | 10 | −173 | 182 | −173 | −97 | −172 | 307 |
| | | 0.3 | 28 | 0.174 | 26 | 0.88 | 21.9 | 79 | 2190 | −173 | −17 | −173 | 126 | −173 | −108 | −172 | 233 |
| | | 0.5 | 26 | 0.106 | 24 | 0.74 | 20.6 | 79 | 2010 | −173 | −36 | −173 | 85 | −173 | −117 | −172 | 180 |
| 3[a] | 0.02 | 1.5 | 25 | 0.044 | 12 | 0.76 | 1.80 | 77 | 141 | 4 | 19 | 4 | 23 | 5 | 28 | 10 | 41 |
| | 0.01 | 1.5 | 25 | 0.071 | 18 | 0.76 | 3.85 | 101 | 408 | −67 | −33 | −67 | −25 | −67 | −53 | −62 | −12 |
| | 0.006 | 1.5 | 26 | 0.078 | 20 | 0.80 | 6.30 | 125 | 855 | −111 | −12 | −109 | 133 | −112 | −67 | −106 | 181 |
| | 0.003 | 1.5 | 35 | 0.159 | 31 | 0.45 | 17.4 | 166 | 4035 | −172 | 219 | −172 | 1071 | −173 | 28 | −171 | 1531 |
| 5[b] | 0.02 | 10 | 48 | 0.055 | 19 | 0.74 | 2.05 | 78 | 164 | 30 | 79 | 64 | 175 | 14 | 37 | 93 | 261 |
| | 0.01 | 10 | 48 | 0.055 | 26 | 0.74 | 2.91 | 113 | 314 | −42 | 17 | −4 | 150 | −55 | −26 | 28 | 275 |
| | 0.006 | 10 | 48 | 0.055 | 31 | 0.74 | 3.78 | 127 | 513 | −96 | −25 | −67 | 142 | −105 | −69 | −42 | 306 |
| | 0.003 | 10 | 48 | 0.055 | 36 | 0.74 | 5.40 | 167 | 1007 | −161 | −77 | −134 | 145 | −167 | −123 | −114 | 382 |

[a] The results for these masses are based on the analytical formulae.

[b] The results of the 5 $M_\odot$ models are based on the full FRANEC evolutionary calculations.

Because we are interested in comparing the C and Si isotopic ratios predicted for the envelopes of many AGB stars characterized by different masses, metallicities, and mass-loss trends, for AGB stars of masses $\leq 3\ M_\odot$ we have used the analytic formulae provided by Straniero et al. (2003, 2006) to obtain the stellar structure parameters needed for the postprocessing code for a large number of models. These formulae were generated by interpolating the results of a set of stellar models based on the Frascati Raphson Newton Evolutionary Code (FRANEC; Straniero et al. 1997) for the evolution of stars from the pre–main-sequence through the AGB phase, including mass loss according to Reimers's (1975) prescription (see below). Our grid of models based on the analytical formulae covers the masses $M = 1.5$, 2, and 3 $M_\odot$ and the metallicities $Z = 0.003$, 0.006, 0.01, and 0.02 (solar). For stars of 5 $M_\odot$, we have used the results of stellar model calculations with the FRANEC code for the same range of metallicities (Vaglio et al. 1998; Straniero et al. 2000). In contrast to the Monash models (§ 3.2), no special algorithms were adopted to handle the discontinuity in the opacity that forms at the base of the convective envelope during TDU. With the Schwarzschild criterion and an appropriately small mass and time resolution, TDU is found to occur for stars with masses as low as 1.5 $M_\odot$ at solar metallicity.

The evolution of an AGB star is dramatically affected by mass loss. A rather large spread of mass-loss rates has been observed (van Loon et al. 1999; Schöier & Olofsson 2001; Whitelock et al. 2003; Winters et al. 2003), typically in the range $10^{-8}$ to $10^{-4}\ M_\odot\ \mathrm{yr}^{-1}$. In spite of much observational and theoretical effort, the mass-loss rates from AGB stars are still not well determined. No clear correlations with stellar mass, luminosity, radius, chemical composition, or any other stellar parameter have been found. The only correlation that has been found is between the period and the luminosity of regular AGB variables. However, differences up to 1 order of magnitude in mass-loss rate are commonly reported for variable stars with similar periods. To evaluate the influence of the mass loss on our predictions of the Si isotopic ratios in C stars, we used a scaled Reimers formula (Reimers 1975),

$$dM/dt\left(M_\odot\ \mathrm{yr}^{-1}\right) = 1.34 \times 10^{-5} \eta L^{3/2} / \left(M T_{\mathrm{eff}}^2\right),$$

where the mass $M$ and luminosity $L$ are in solar units, $T_{\mathrm{eff}}$ is in K, and $\eta$ is a scale factor. Owing to the large uncertainty of the AGB mass loss, we have varied the $\eta$ parameter over a wide range of values, namely, 0.1, 0.3, 0.5, 1.5, and 10.

In Table 1 we report, for each model calculation, the total number of TDU episodes experienced by the AGB star, the total mass dredged up by TDU, the number of TDU episodes at which the C/O ratio in the envelope becomes higher than unity, the mass of the envelope remaining after the last TDU, and the final C/O ratio. We also list the C and Si isotopic ratios in the envelope at the

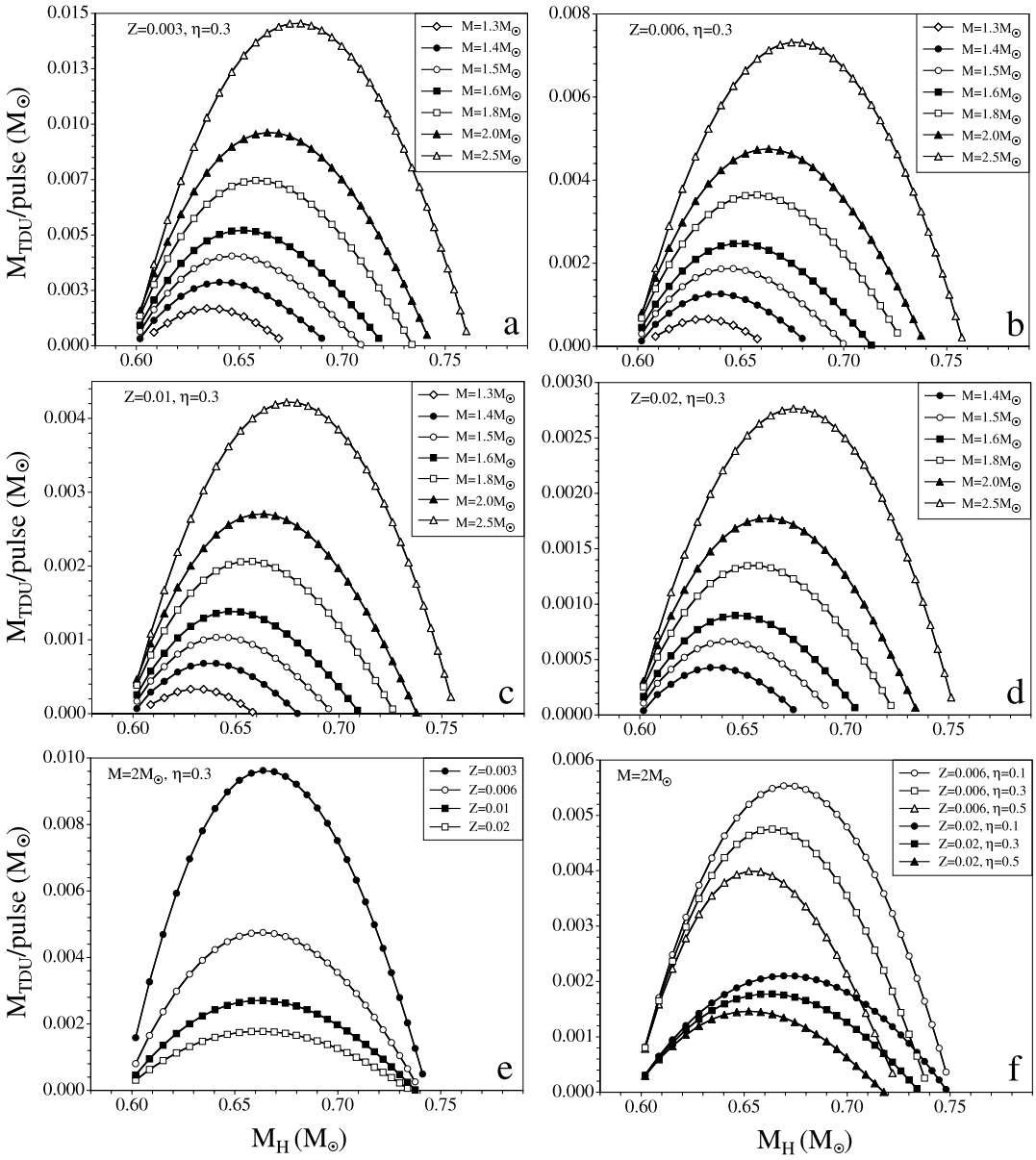


FIG. 4.—Model calculations, based on the FRANEC code, of the mass dredged up into the envelope of AGB stars following each thermal pulse during the TP-AGB phase. The dredged-up mass is plotted against the location of the H-burning shell in solar mass units for different stellar masses, metallicities, and choices of the Reimers parameter for the mass loss. As can be seen, the dredged-up mass increases with (*a*–*d*) increasing mass, (*e*) decreasing metallicity, and (*f*) decreasing mass loss.

time the C/O ratio reaches unity and after the last TDU. As can be seen in the table, we achieve TDU in all the models considered, and all models except the 1.5 $M_{\odot}$ model with solar metallicity and $\eta = 0.5$ achieve C > O by the end of the last TDU. As shown by previous AGB calculations (Boothroyd & Sackmann 1988a), the efficiency of the TDU, i.e., the number of TDU episodes and the total dredged-up mass, increases with increasing initial mass of the star and with decreasing metallicity. The mass-loss rate also influences the TDU efficiency. Higher choices of Reimers parameter $\eta$ result in a reduction of the number of TDU episodes, as well as in a decrease in the total dredged-up mass. The reason for this is the fact that the dredged-up mass is a function of the mass of the envelope, which in turn is determined by the mass-loss law. The mass dredged up during each TDU episode increases, reaches a maximum, and then decreases, until the TDU ceases when the mass of the envelope decreases below a certain value, around 0.4 $M_{\odot}$ for stellar models of mass 1.5 $M_{\odot}$ and around 0.7 $M_{\odot}$ for stellar models of mass 3 $M_{\odot}$ (Straniero et al. 2003, 2006). Figures 4*a*–4*f* show the dredged-up mass per TDU episode with increasing pulse number as a function of the mass location of the H-burning shell for different initial stellar masses and for a few selected values of metallicity and Reimers parameter. As H and He burning proceeds throughout the TP-AGB phase, increasing amounts of H are turned into He and of He are turned into C and O. The mass coordinate of the H-burning shell thus increases with pulse number. At the same time the star loses mass. However, TDU stops when a substantial fraction of the envelope mass is still present, and this affects the composition of the dust grains produced in the wind of these stars. The grains formed at any given time carry the signature of the cumulative TDU episodes that had occurred up to that time. Since mass loss and grain formation continue after cessation of the TDU, according to the evolution models at least a third of SiC grains produced by a given star should form with the envelope composition being that after

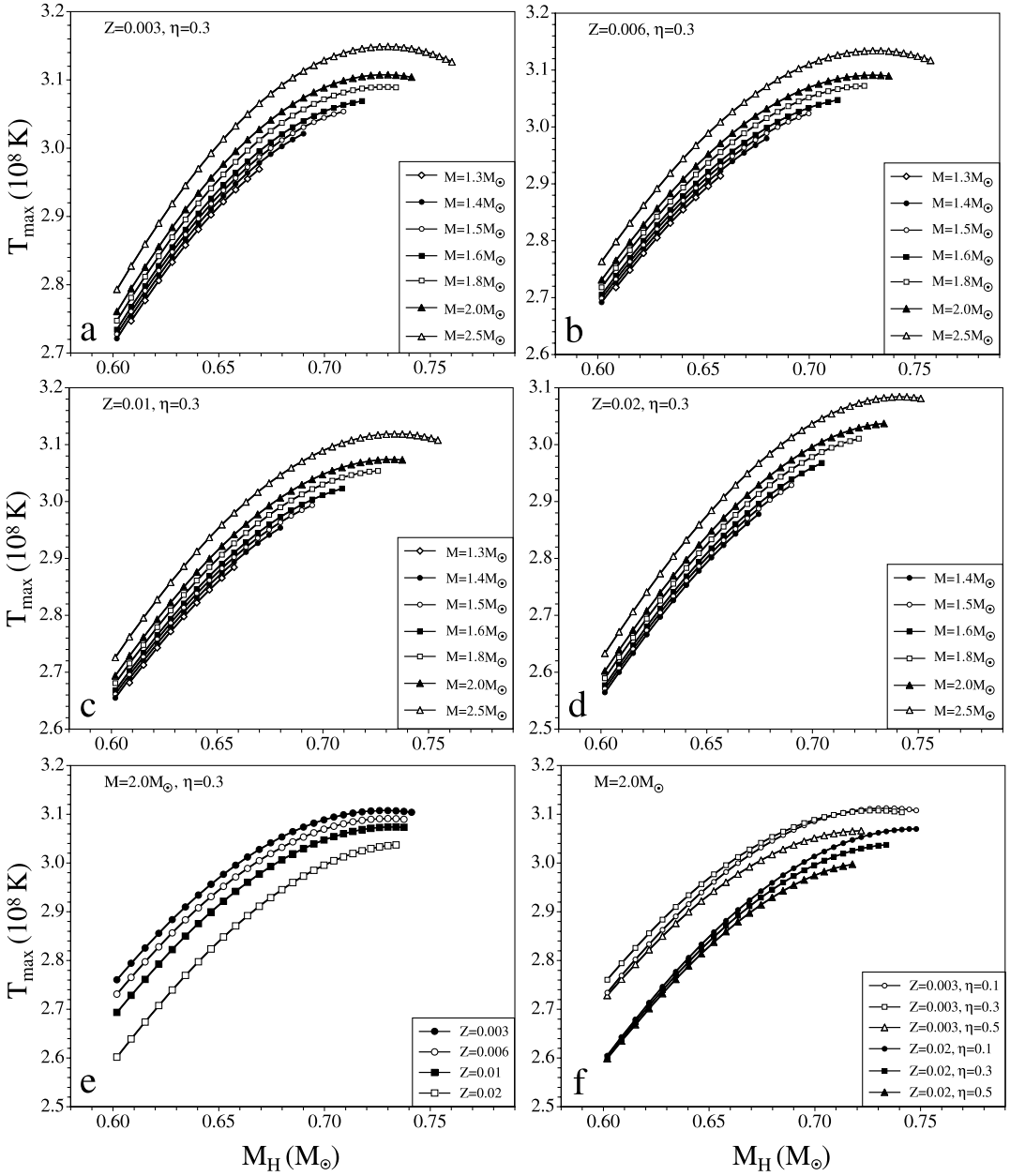


FIG. 5.—Model calculations of the maximum temperature reached in the convective region of subsequent thermal pulses. As in Figs. 4*a*–4*f*, the temperature is plotted against the mass location of the H-burning shell for different masses, metallicities, and mass loss. Similar to the dredged-up mass, the maximum temperature increases with (*a*–*d*) increasing mass, (*e*) decreasing metallicity, and (*f*) decreasing mass loss.

the last TDU episode. Figures 5*a*–5*f* show the evolution of the maximum temperature in the convective zone powered by the TP as function of the mass location of the H-burning shell for different masses and for a few selected values of metallicity and Reimers parameter. The temperature is an important input parameter for the postprocessing code. As can be seen from the plots, the maximum temperature increases with increasing stellar mass (Figs. 5*a*–5*d*), decreasing metallicity (Fig. 5*e*), and decreasing mass loss (Fig. 5*f*).

Whereas the stellar structure models (including the analytical formulae) used the solar abundances compiled by Anders & Grevesse (1989), the postprocessing code that computed the C/O as well as the C and Si isotopic ratios used as initial C and O abundances the solar values reported by Allende Prieto et al. (2001, 2002; see also Asplund 2005). These abundances are by factors of 1.5 and 1.9 lower than the Anders & Grevesse (1989) values. This means that the solar metallicity is not 0.02 anymore, as it is with the Anders & Grevesse abundances, but close to 0.0133. In this paper we label the different models according to the global metallicities used for the stellar structure calculations ($Z = 0.02$, 0.01, 0.006, and 0.003), but it has to be understood that the metallicities used in the nucleosynthesis calculations are different. The expected effect of the new, lower C and O abundances on the stellar structure parameters would be very similar to that of decreasing the metallicity in the stellar models (or the analytical formulae yielding the structure parameters) from $Z = 0.02$ to 0.0133, etc. To first order the physical parameters are sensitive to $Z$ rather than the exact distribution of the elements in the "metals."

The new abundance values facilitate the formation of carbon stars at solar metallicity, because the initial O abundance in the envelope is lower while dredge-up of newly synthesized $^{12}$C is

TABLE 2
METALLICITY VALUES AND INITIAL Si ISOTOPIC RATIOS OF THE STELLAR MODELS

| Parameter | Torino Models | | | | Monash Models | | |
|---|---|---|---|---|---|---|---|
| [Fe/H] | 0 | −0.301 | −0.523 | −0.824 | 0 | −0.398 | −0.699 |
| $Z_{\rm structure}$ | 0.02 | 0.01 | 0.006 | 0.003 | 0.02 | 0.008 | 0.004 |
| $Z_{\rm nucleosynthesis}$ | 0.0133 | 0.0072 | 0.0045 | 0.0024 | 0.02 | 0.0083 | 0.0044 |
| $\delta^{29,30}{\rm Si}_{\rm init}$ | 0 | −67‰ | −113‰ | −173‰ | 0 | −88‰ | −149‰ |

not affected by the C and O abundances. Another consequence is that $^{12}C/^{13}C$ ratios in the envelope are higher with the new abundances, whereas the Si isotopic ratios remain essentially unaffected. For lower metallicities, the initial composition of the star in the models is set by scaling the solar abundance distribution to the metallicity (Fe abundance) of the star for all nuclei except nuclei such as $^{16}O$, $^{20}Ne$, $^{24}Mg$, and $^{28}Si$, whose initial abundances are enhanced relative to Fe and the other isotopes. The enhancement trends for these nuclei were deduced from observations of F and G stars belonging to the Galactic thin disk (McWilliam 1997; Reddy et al. 2003). The final metallicities reflecting the choice of the new C and O solar abundances and the enhancement of the above nuclei are given in Table 2. Since these changes do not involve Fe, the metallicities expressed by [Fe/H] are the same for the stellar structure and nucleosynthesis calculations.

The Torino postprocessing code has a network of neutron captures on 404 isotopes from C to Po, the termination point of the $s$-process, and $\beta$-decays for all unstable nuclei involved. For a selected network of nuclei up to Mg, $\alpha$-capture reactions are also computed, among them the neutron source reactions. Reaction rates for neutron production have been taken from Denker et al. (1995) for the $^{13}C(\alpha, n)^{16}O$ reaction, which is roughly 40% slower than the NACRE rate (Angulo et al. 1999), and from Käppeler et al. (1994) for the $^{22}Ne(\alpha, n)^{25}Mg$ reaction, excluding the contribution of the elusive resonance at 633 keV. The latter rate is roughly the same as that given in the NACRE compilation. Neutron-capture cross sections and decay rates are tabulated at two different temperatures: 8 keV, typical for the activation of the $^{13}C(\alpha, n)^{16}O$ reaction, and 23 keV, typical for the activation of the $^{22}Ne(\alpha, n)^{25}Mg$ reaction. Rates for $(n, \gamma)$ reactions on stable nuclei are updated to include the latest estimates (Bao et al. 2000). More details about $(n, \gamma)$ reactions on unstable nuclei, about the $(n, \alpha)$ and $(n, p)$ reaction rates, and about decay rates can be found in Gallino et al. (1998).

Neutron captures on the Si isotopes proceed via the chain $^{28}Si(n, \gamma)^{29}Si(n, \gamma)^{30}Si(n, \gamma)^{31}Si$. An additional important contribution to the abundance of $^{30}Si$ derives from the reaction $^{33}S(n, \alpha)^{30}Si$, which has a large cross section, 181 mbarn at 30 keV (Schatz et al. 1995). In our nucleosynthesis calculations we used two different sets of neutron-capture cross sections for the Si isotopes. These are listed in Table 3 for temperatures of 8, 23, and 30 keV, usually given in the literature. Given in the table are the values $\sigma = \langle\sigma(v)v\rangle/v(30\ {\rm keV})$, where $v$ is the relative velocity and angle brackets indicate the Maxwellian average for a temperature corresponding to the energy considered. Also given in Table 3, at 30 keV, are the errors as percentage standard deviations and the ratios of the values of one set to those of the other. The first set of values was taken from the compilation of neutron-capture cross sections by Bao et al. (2000) and is virtually identical to the set of values used in the calculations reported by Lugaro et al. (1999). These values are based on the old experimental data of Boldeman et al. (1975). A more recent experimental determination of the cross sections using a time-of-flight technique has been presented by Guber et al. (2003). For $^{28}Si$ the new cross section is about half as large as the old one, and for $^{29}Si$ the cross section is almost unchanged, whereas for $^{30}Si$ there is a huge change, with the new cross section being from 6.8 to 3.6 times smaller than the old one at the temperatures of interest [$(2.5-3.5)\times10^8$ K]. The cross section of $^{30}Si(n, \gamma)^{31}Si$ has also been measured using the activation technique (Beer et al. 1992). These authors give a value, at 25 keV, that is 1.65 times higher than that measured by Guber et al. (2003), but still much lower than that in the compilation by Bao et al. (2000).

The silicon isotopic ratios computed with the Guber et al. (2003) neutron-capture cross sections show the following features with respect to calculations performed using the values of Bao et al. (2000). Because the $^{28}Si(n, \gamma)^{29}Si$ cross section of the second (Guber et al.) set is lower than that of the first set, the final

TABLE 3
NEUTRON-CAPTURE CROSS SECTIONS $\sigma$ FOR THE Si ISOTOPES

| | Bao et al. (2000) | | | | Guber et al. (2003) | | | |
|---|---|---|---|---|---|---|---|---|
| Isotope | 8 keV | 23 keV | 30 keV | Standard Deviation at 30 keV (%) | 8 keV | 23 keV | 30 keV | Standard Deviation at 30 keV (%) |
| $^{28}Si$ | 0.32 | 2.35 | 2.90 | 10.3 | 0.25 | 1.12 | 1.42 | 9.1 |
| $^{29}Si$ | 6.67 | 8.87 | 7.90 | 11.4 | 5.43 | 8.08 | 7.56 | 12.6 |
| $^{30}Si$ | 31.23 | 8.91 | 6.50 | 9.2 | 4.59 | 2.01 | 1.82 | 18.1 |
| | Ratio Guber/Bao | | | | | | | |
| $^{28}Si$ | 0.78 | 0.48 | 0.49 | | | | | |
| $^{29}Si$ | 0.81 | 0.91 | 0.96 | | | | | |
| $^{30}Si$ | 0.15 | 0.23 | 0.28 | | | | | |

NOTE.—The cross sections given are $\sigma = \langle\sigma(v)v\rangle/v(30\ {\rm keV})$ (see text).

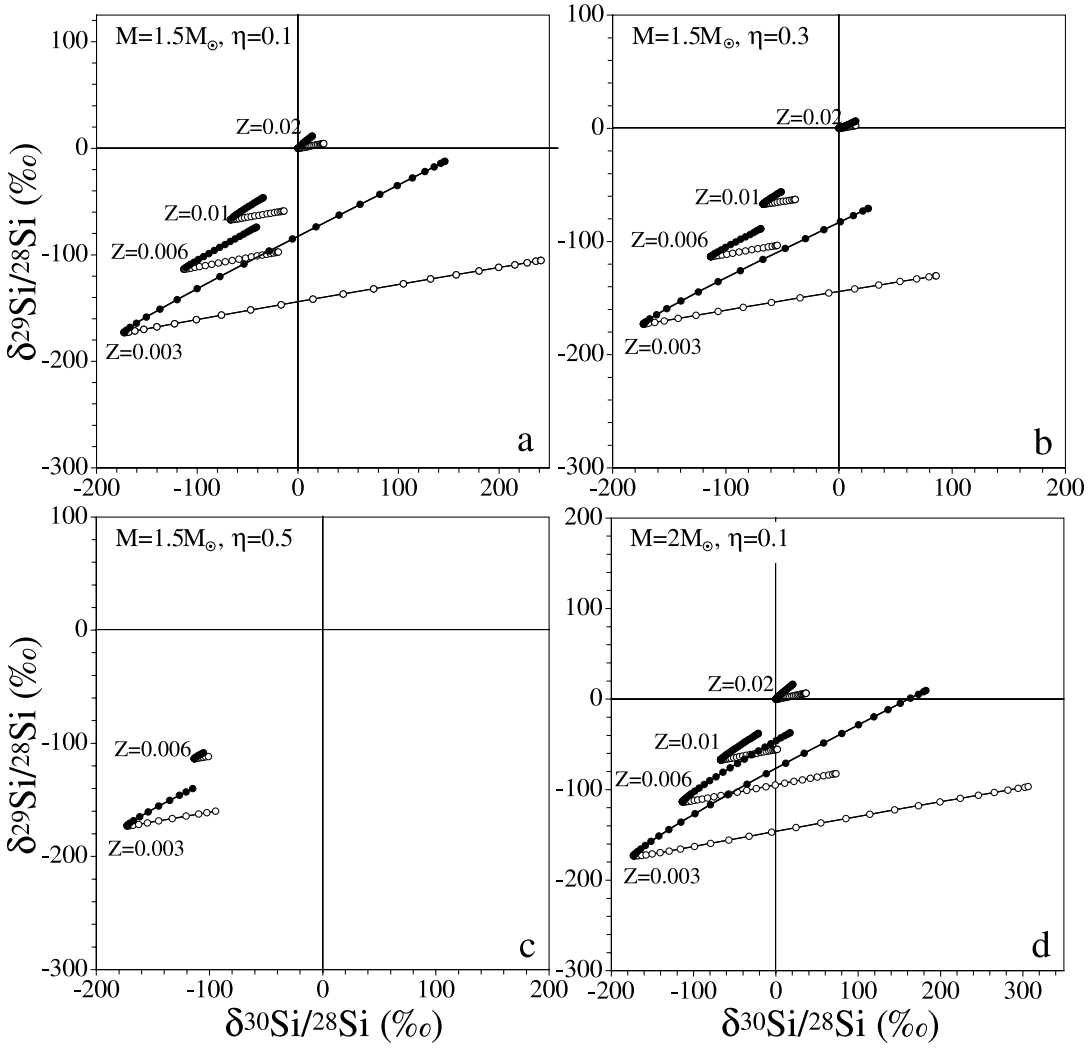


FIG. 6.—Theoretical predictions (based on the Torino model and the FRANEC code) of the evolution of the Si isotopic ratios in the envelope of AGB stars during successive thermal pulses. As in Fig. 2, Si isotopic ratios are displayed as $\delta$-values. Predictions are plotted for different stellar masses, metallicities, and Reimers parameters. Solid circles are results based on the Bao et al. (2000) neutron-capture cross sections, and open circles are results based on the Guber et al. (2003) cross sections. In all cases shown, except for the $M = 5\,M_{\odot}$ case, noticeable changes in the Si isotopes occur only after the star has become a carbon star, i.e., when C > O. In (*h*) the $M = 5\,M_{\odot}$ case, the evolution of the Si isotopes with C < O is indicated by solid lines without any symbols. Even in this case, most changes occur when C > O. All results are for the "standard" $^{13}$C pocket (Gallino et al. 1998; Lugaro et al. 2003b).

$^{29}$Si/$^{28}$Si ratios are lower, the exact difference depending on the stellar model considered. On the other hand, because the $^{30}$Si($n$, $\gamma$)$^{31}$Si cross section is much lower, the final $^{30}$Si/$^{28}$Si ratios predicted on the basis of the Guber et al. (2003) data are higher. Also in this case, the exact difference is a function of the stellar model considered. In a three-isotope plot such as those of Figures 6*a*–6*h* these differences translate into a change in the slope of the approximately linear function that describes the evolution of the Si isotopic ratios at the surfaces of AGB stars during repeated TDUs. This slope is always much smaller in the models computed with the Guber et al. (2003) cross sections than those computed with the Bao et al. (2000) cross sections. For example, in the case of a 2 $M_{\odot}$ star of solar metallicity (Figs. 6*d*–6*f*) the slope of the evolution line of the Si ratios expressed in $\delta$-values changes from 0.82 (with Bao et al.) to 0.17 (with Guber et al.). For a 3 $M_{\odot}$ star of metallicity $Z = 0.003$ (Fig. 6*g*) the slope changes from 0.42 to 0.08. In any case, it is important to note that the adopted neutron-capture cross sections do not fundamentally change the major features of the evolution of the Si isotopic ratios in AGB stars. In particular, for stars of mass $\leq 3\,M_{\odot}$ and solar metallicity the initial Si isotopic ratios are only slightly changed by neutron capture in AGB stars, no matter which set of cross sections is used, and the slope of the evolution line in a three-isotope plot is less than unity for any choice of stellar model and cross sections.

For lower than solar metallicities, we calculated the initial abundance of $^{28}$Si by applying a factor that increases linearly with decreasing metallicity, so that at [Fe/H] = −1, [Si/Fe] = +0.1 (Reddy et al. 2003). The initial abundances of $^{29}$Si and $^{30}$Si, on the other hand, were not modified and were assumed to scale with the Fe abundance. With these choices the initial $^{29}$Si/$^{28}$Si and $^{30}$Si/$^{28}$Si ratios decrease linearly with decreasing [Fe/H] of the star, reaching values 7%, 11%, and 17% lower than the solar ratios (i.e., $\delta$-values of −67‰, −113‰, and −173‰) at $Z = 0.01$, 0.006, and 0.003, respectively (see Table 2). These assumed values do not agree with the results of GCE calculations, which take into account metallicity-dependent Si isotope yields from SNe II (Timmes & Clayton 1996).

The Si isotopic results of the Torino models are shown in Figures 6*a*–6*h*. They are plotted as $\delta$-values in a three-isotope plot, as in Figure 2. Individual symbols in the plots indicate ratios after individual TPs and TDUs in the stars' envelopes for C > O. Isotopic ratios in the envelope with C < O are given only as black

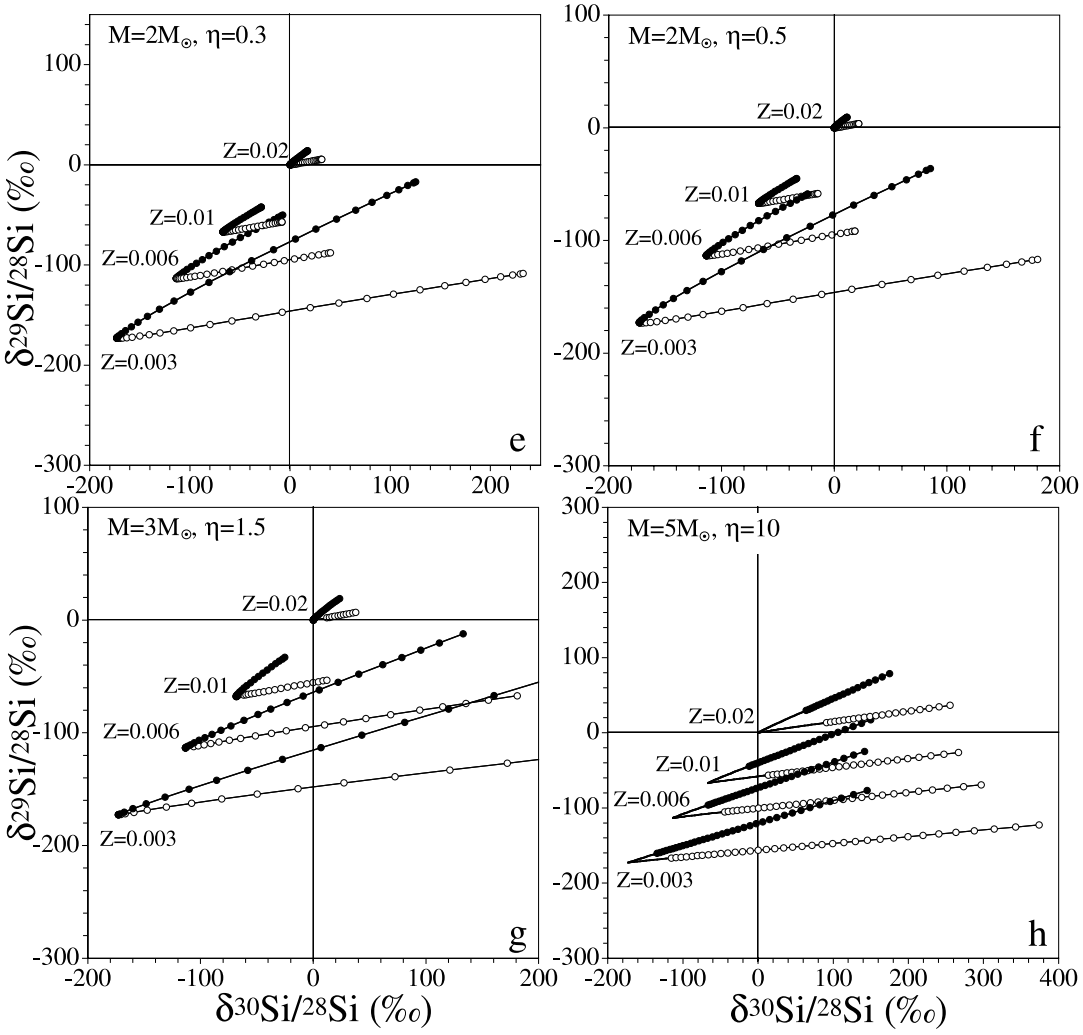


FIG. 6.—*Continued*

lines without symbols. In all stellar models, with the exception of $M = 5\ M_{\odot}$, the changes in the Si isotopic ratios are negligible as long as the envelope is O-rich (C < O), and only after the stars turn into carbon stars does the TDU lead to significant enrichments in the heavy Si isotopes (Figs. 6*a*–6*g*). It is only in the 5 $M_{\odot}$ model (Fig. 6*h*) that there are noticeable changes already during the O-rich evolution of the envelope. In stars of mass $\leq 3\ M_{\odot}$ and solar metallicity the temperature at the base of the convective pulses reaches $3 \times 10^8$ K during the final thermal pulses (Fig. 5*d*). At this temperature the $^{22}$Ne($\alpha$, $n$)$^{25}$Mg reaction is marginally activated, and the changes in the Si isotopic ratios in these stars are small. In stars of higher mass or lower metallicity the temperature at the base of the convective pulse is higher. For example, for a 5 $M_{\odot}$ star of solar metallicity it reaches $3.6 \times 10^8$ K, and for a 3 $M_{\odot}$ star of metallicity $Z = 0.003$ it reaches $3.4 \times 10^8$ K. In these cases the Si isotopic ratios are significantly modified. This is clearly demonstrated in Figure 6, where the enrichments of the heavy Si isotopes increase with increasing mass and decreasing metallicity.

Of course, other stellar parameters, such as the fraction of material in the TP that has been exposed to the previous TP, the amount of TDU, and the mass of the envelope, also influence the Si isotopic composition. For example, even though the model of a 5 $M_{\odot}$ star of solar metallicity reaches a higher temperature at the base of the TP than the stellar model with 3 $M_{\odot}$ and $Z = 0.003$, the final $\delta^{30}$Si value in the envelope is much higher in the 3 $M_{\odot}$ than in the 5 $M_{\odot}$ star. This is due to the fact that the amount of material dredged up in the 3 $M_{\odot}$ star with $Z = 0.003$ is about 3 times as high as that in the 5 $M_{\odot}$ star of solar metallicity. Moreover, the overlap factor (the fraction of material in a given convective thermal pulse that is contained in the subsequent thermal pulse) in a 5 $M_{\odot}$ star is about 1/3, compared to about 1/2 in the lower mass stars. The envelope mass depends on the mass loss and thus in the Torino models on the Reimers parameter $\eta$. As can be seen in the 1.5 and 2 $M_{\odot}$ models, the isotopic enhancements decrease with increasing mass-loss parameter (Figs. 6*a*–6*f*), but the effect is much more pronounced for the lower mass.

The Si isotopes are mostly affected by the $^{22}$Ne neutron source and only minimally by the $^{13}$C source. Therefore, the changes in the Si isotopic ratios in the envelope do not depend very much on the assumed strength of the $^{13}$C pocket. Figures 7*a*–7*f* show the final Si isotopic ratios in the envelope reached after the final TP for different assumed $^{13}$C pockets relative to the standard pocket, which best reproduces the *s*-process elements in the solar system (see, e.g., Lugaro et al. 2003a). The assumed pockets range from d12, a factor of 12 weaker than the standard pocket, to u2, a factor of 2 stronger (see Fig. 7*a*). The fact that isotopic shifts in many cases are higher for weak $^{13}$C pockets than for the standard pockets is explained by the complex interplay between temperature dependences of the cross sections of various neutron poisons.

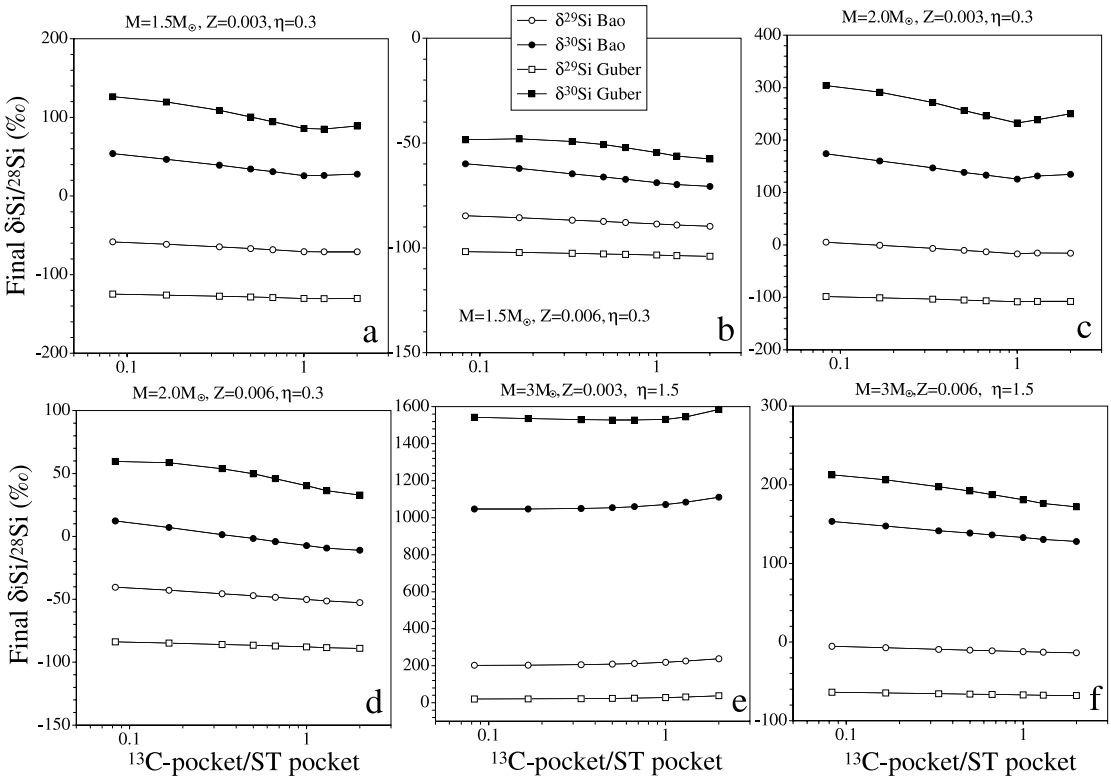


FIG. 7.—Predicted final envelope Si isotopic ratios reached at the end of the TP-AGB phase plotted as functions of the strength of the $^{13}$C pocket for different masses, metallicities, and Si neutron-capture cross sections. The strength of the $^{13}$C pocket ranges from a factor of 12 smaller to a factor of 2 larger than that of the "standard" (ST) pocket (Lugaro et al. 2003b). Because the Si isotopes are mostly affected by neutrons released from the $^{22}$Ne source during the TP, the strength of the $^{13}$C pocket has only a minor influence on the final Si isotopic ratios.

The choice of neutron-capture cross sections of the Si isotopes plays an important role for the evolution of the Si isotopic ratios in the stars' envelopes. Whereas the cross sections of Bao et al. (2000) result in shifts along lines with slopes between ~0.4 and 0.8 in a three-isotope $\delta$-value Si plot, the Guber et al. (2003) cross sections lead to trajectories with slopes of ~0.18 (Figs. 6*a*–6*h*). As a consequence, the final shifts in $\delta^{29}$Si are smaller and the shifts in $\delta^{30}$Si are larger for the models using the Guber cross sections than those using the Bao cross sections (Figs. 7*a*–7*f* and Table 1).

### 3.2. *Monash Models*

To model the nucleosynthesis in AGB stars, we have also computed a series of stellar structure models using the Monash version of the Mount Stromlo Stellar Structure program (Frost & Lattanzio 1996; Karakas et al. 2002). We calculated models with masses between 1 and 6.5 $M_{\odot}$ at $Z = 0.02$ and between 1 and 6 $M_{\odot}$ at $Z = 0.008$ and $Z = 0.004$. The structure of each model was computed from the zero-age main sequence, through all intermediate stages including the core He flash in low-mass models, to near the end of the thermally pulsing AGB phase. Mass loss on the first giant branch was included using the Reimers (1975) mass-loss prescription with the parameter $\eta = 0.4$; on the AGB we used the mass-loss prescription of Vassiliadis & Wood (1993, hereafter VW93), which accounts for a final superwind phase. We computed the evolution and structure of a second 5 $M_{\odot}$, $Z = 0.02$ model for comparison that has the Reimers mass-loss rate on the AGB, with $\eta = 3.5$, instead of that of VW93. This case is discussed further below.

The parameters for the different models are given in Table 4. We find the TDU to occur in all models with masses above 2.25 $M_{\odot}$ for $Z = 0.02$ and above 1.5 $M_{\odot}$ at $Z = 0.008$ and 0.004. More details regarding these calculations can be found in Karakas et al. (2002) and Karakas (2003). We note that the amount of TDU is sensitive to the input physics and the initial composition and mass of the model, as well as to the treatment of convective borders (Frost & Lattanzio 1996; Mowlavi 1999) and the mixing-length theory parameter, $\alpha$, which determines the efficiency of convection affecting the depth of the TDU (Boothroyd & Sackmann 1988b). The inclusion of convective overshoot is also required in some cases for efficient TDU (Mowlavi 1999; Herwig 2000), and reaction rates have also been found to be important (Herwig & Austin 2004). In the structure calculations, we use the standard mixing-length theory, with $\alpha = 1.75$, and do not include convective overshoot, in the usual sense. We do search for a neutral border to the base of the convective envelope, as described in detail by Lattanzio (1986), and this has been shown to increase the efficiency of the TDU (Frost & Lattanzio 1996).

Silicon carbide grains only form in an environment where C/O > 1, so we limit the following discussion to those models that became carbon stars. At $Z = 0.02$, this includes the 2.5, 3, and 3.5 $M_{\odot}$ models with VW93 mass loss. The 4 and 5 $M_{\odot}$ models do not become carbon-rich (cf. Table 4), simply because the amount of matter dredged up over the course of the AGB phase is not enough to enrich the envelope sufficiently to achieve C > O. A reduction in the initial $^{16}$O solar abundance from the Anders & Grevesse (1989) value, which we use, to that found by Allende Prieto et al. (2001) used in the Torino models, would change these results considerably, because the conditions for producing a carbon star would be more easily achieved. However, the 5 $M_{\odot}$ model with Reimers mass loss does become carbon-rich, because there are more TDUs, which leads to more mass being dredged up into the envelope. The case with VW93 mass loss also has a shorter lifetime and few thermal pulses (24) compared to the

TABLE 4
PARAMETERS OF DIFFERENT STELLAR EVOLUTION MODELS OBTAINED FROM THE MONASH STELLAR CODE

| Mass | $Z$ | TDU Episodes | TDU Mass ($M_\odot$) | TDU with C/O > 1 | Final C/O | $^{12}C/^{13}C$ at C/O = 1 | Final $^{12}C/^{13}C$ | $\delta^{29}Si$ at C/O = 1 | Final $\delta^{29}Si$ | $\delta^{30}Si$ at C/O = 1 | Final $\delta^{30}Si$ |
|---|---|---|---|---|---|---|---|---|---|---|---|
| 1.5..... | 0.004 | 6 | 0.0089 | 1 | 1.14 | 142 | 142 | −144 | −144 | −142 | −142 |
| 1.75..... | 0.008 | 7 | 0.0128 | 1 | 1.00 | 103 | 103 | −81 | −81 | −79 | −79 |
| 1.75..... | 0.004 | 8 | 0.0240 | 4 | 2.21 | 123 | 277 | −144 | −135 | −142 | −130 |
| 1.9..... | 0.008 | 8 | 0.0262 | 2 | 1.31 | 105 | 137 | −81 | −77 | −79 | −74 |
| 1.9..... | 0.004 | 10 | 0.0408 | 6 | 3.15 | 125 | 401 | −144 | −123 | −144 | −114 |
| 2.5..... | 0.02 | 9 | 0.0208 | 0 | 0.80 | ... | 67 | ... | 8 | ... | 10 |
| 2.5..... | 0.008 | 18 | 0.1069 | 10 | 3.34 | 106 | 364 | −81 | −30 | −79 | −2 |
| 2.5..... | 0.004 | 24 | 0.1911 | 20 | 8.12 | 123 | 1061 | −144 | 12 | −142 | 119 |
| 3..... | 0.02 | 16 | 0.0796 | 4 | 1.41 | 84 | 118 | 13 | 27 | 17 | 39 |
| 3..... | 0.008 | 26 | 0.2108 | 19 | 4.99 | 100 | 519 | −78 | 69 | −76 | 181 |
| 3..... | 0.004 | 25 | 0.2059 | 20 | 7.41 | 113 | 896 | −141 | 116 | −138 | 378 |
| 3.5..... | 0.02 | 18 | 0.1066 | 6 | 1.56 | 82 | 126 | 22 | 52 | 32 | 85 |
| 4..... | 0.02 | 18 | 0.0551 | 0 | 0.99 | ... | 77 | ... | 40 | ... | 74 |
| 4..... | 0.008 | 21 | 0.0856 | 9 | 2.00 | 79 | 28 | −55 | 28 | −35 | 143 |
| 5..... | 0.02 | 24 | 0.0494 | 0 | 0.77 | ... | 8 | ... | 44 | ... | 87 |
| 5..... | 0.02[a] | 38 | 0.1023 | 12 | 1.71 | 11 | 16 | 59 | 137 | 121 | 302 |
| 5..... | 0.004 | 80 | 0.2250 | 3 | 2.10 | 6 | 11 | 360 | 419 | 854 | 996 |

[a] Model with Reimers mass loss on the AGB with $\eta = 3.5$.

model with Reimers mass loss (38). Efficient hot bottom burning (HBB), a condition in which the convective envelope reaches into the H-burning zone (Lattanzio et al. 1996, 1997, 2000; Frost et al. 1998; Lattanzio & Forestini 1999), converts the carbon dredged to the stellar surface to $^{14}N$ in the CNO cycle, which prevents the formation of a carbon-rich environment, and this is what happens in the 6 and 6.5 $M_\odot$ solar composition models with VW93 mass loss.

In the lower than solar metallicity models, we present results for the 1.75, 1.9, and 3 $M_\odot$ $Z = 0.008$ models and the 1.5, 1.9, 2.5, and 3 $M_\odot$ $Z = 0.004$ models (Table 4). All models between 1.5 and 6 $M_\odot$ become carbon-rich at some stage during the TP-AGB phase. In the lower mass models, with $M < 4\ M_\odot$, efficient TDU mixing causes the envelope composition to become carbon-rich, while in the more massive models, the complex interplay between very efficient TDU, mass loss, and HBB destroying some $^{16}O$ results in the models becoming carbon-rich during the last few thermal pulses. These models correspond to optically obscured luminous carbon-rich AGB stars, similar to those modeled by Frost et al. (1998) and observed by van Loon et al. (1998).

To calculate the nucleosynthesis in detail we have used a post-processing algorithm that calculates abundance changes owing to nuclear reactions and time-dependent diffusive convective mixing in all convective regions (Cannon 1993; Lugaro et al. 2004). The nucleosynthesis network is based on 74 nuclear species, 59 nuclei from neutrons and protons up to sulfur and another 14 nuclei around the iron group. There is also an additional particle, $g$, for accounting for the number of neutron captures occurring on nuclei beyond $^{61}Ni$, which simulates the $s$-process as a neutron sink. See Lugaro et al. (2004) for more details. All proton, $\alpha$, and neutron captures and $\beta$-decays involving the species listed above are included in the nuclear network, summing up to 506 reactions. This contrasts with the Torino postprocessing code, which computes only neutron captures and $\beta$-decays, but on a much larger number of nuclei (from C to Po), and $\alpha$-captures for nuclei up to Mg. The bulk of the reaction rates are taken from the 1991 update of the REACLIB Data Tables (Thielemann et al. 1986). The reaction rates have been updated using the latest experimental results; see Lugaro et al. (2004) for details. Some differences are present in the nucleosynthesis calculations presented in this work. Notably, we use the NACRE rates (Angulo et al. 1999) for the NeNa, MgAl chains and the $^{22}Ne(\alpha, n)^{25}Mg$ and $^{22}Ne(\alpha, \gamma)^{26}Mg$ reactions. Of relevance for this study are the neutron-capture cross sections used for the reactions involving the silicon isotopes, and these are from Beer et al. (1992). They are essentially the same as those in the Bao et al. (2000) compilation.

Unlike for the Torino models, the initial abundances used in the postprocessing calculations are the Anders & Grevesse (1989) values for the $Z = 0.02$ models, the same as those used for the stellar structure calculations. For the $Z = 0.008$ and $Z = 0.004$ models, we calculate initial abundances in a similar way as in the Torino models: we scale the solar abundances of Anders & Grevesse to the metallicity of the star for all nuclei except the $\alpha$ nuclei (i.e., $^{12}C$, $^{16}O$, $^{20}Ne$, $^{24}Mg$, $^{28}Si$, and $^{32}S$), whose initial abundances are enhanced according to the enhancements observed in thin- and thick-disk stars (Reddy et al. 2003). The resulting global metallicity ($Z$) values are shown in Table 2. The initial Si isotopic ratios, $^{29}Si/^{28}Si$ and $^{30}Si/^{28}Si$, used in the lower than solar metallicity models are less than the solar isotopic values, and for $Z = 0.008$ and $Z = 0.004$ the change, calculated in exactly the same way as for the Torino models, is −88‰ and −149‰, respectively (Table 2).

In Table 4 we present, for each solar composition model that became carbon-rich, and for the selected set of $Z = 0.008$ and $Z = 0.004$ models, information relevant for the formation of SiC grains. In particular, we list the total number of TDU episodes, the total mass dredged up by the TDU, the number of TDU episodes required to turn the model star into a carbon star, and the final C/O ratio. We also list the C and Si isotopic ratios in the envelope at the time the C/O ratio reaches unity and after the last TDU episode. The evolution of the Si isotopic ratios in the star's envelope during TDU for the different models is shown in Figures 8*a*–8*f* in the same way as for the Torino models in Figure 6. Again, solid data points indicate compositions after individual TDUs for C > O in the envelope, and thin lines, the evolution of the Si isotopes for C < O. As for the Torino models, significant changes in the Si isotopic ratios in the envelope in O-rich stars (C < O) occur only for the intermediate masses 4 and 5 $M_\odot$ (Figs. 8*e* and 8*f*).

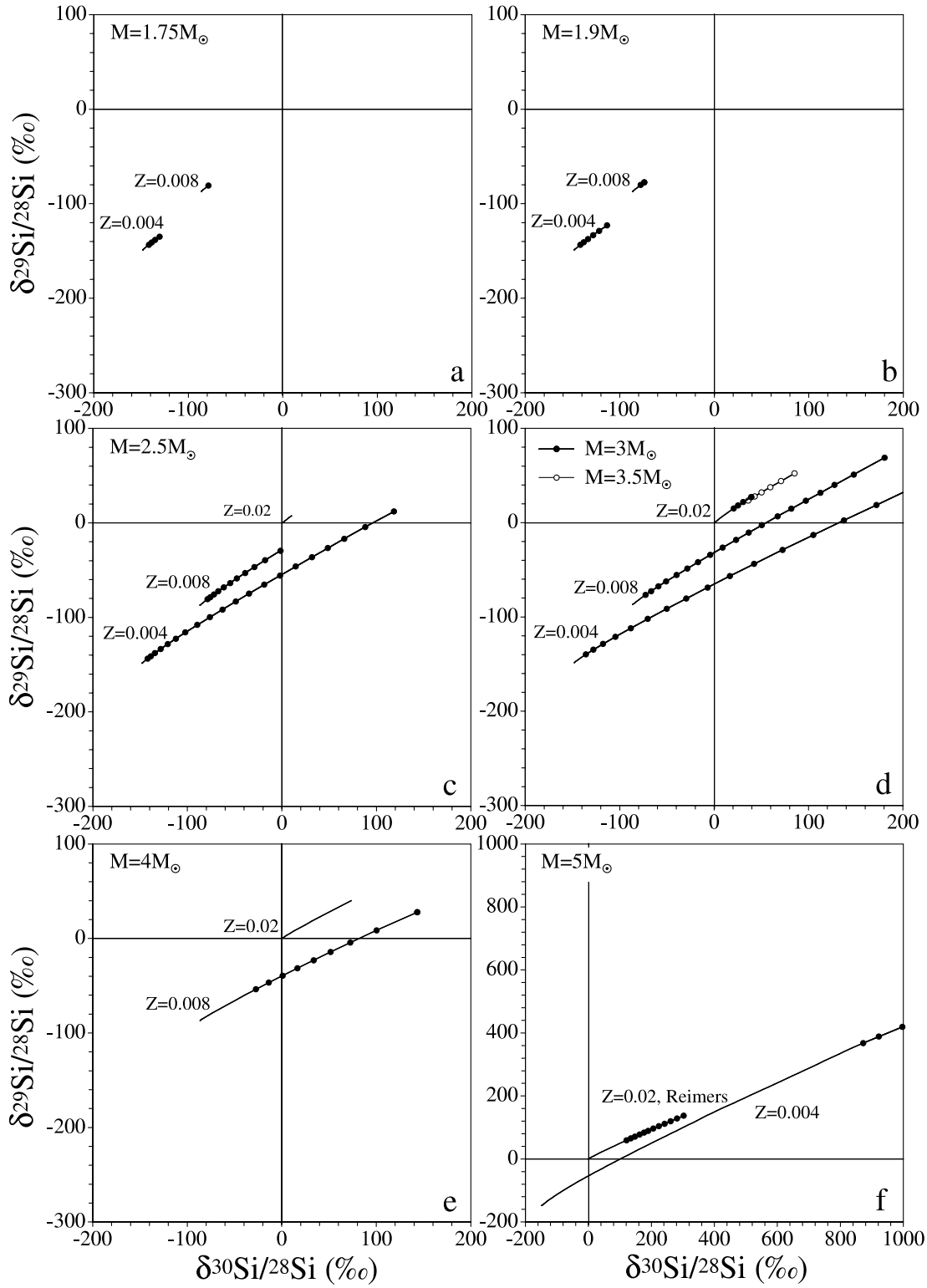


FIG. 8.—Theoretical predictions (based on the Monash model) of the evolution of the Si isotopic ratios in the envelope of AGB stars during successive thermal pulses. Si isotopic ratios are displayed as $\delta$-values. Predictions are plotted for different masses and metallicities. Lines without symbols indicate the evolution of the Si isotopes in the envelope with C $<$ O, and lines with symbols indicate the evolution with C $>$ O, i.e., after the star becomes a carbon star. For low-mass ($M \leq 3.5\ M_{\odot}$) stars, most of the Si isotopic shifts occur while the star is a carbon star, similar to what is found by the Torino models (Fig. 6). Only for the intermediate-mass stars with $M = 4\ M_{\odot}$ and $M = 5\ M_{\odot}$ do we see major Si isotopic shifts in stars with an O-rich (C $<$ O) envelope.

### 3.3. *Comparison of the Torino and Monash Models*

It is not quite straightforward to compare the two sets of models. First of all, the model sets have only the solar ($Z = 0.02$) composition in common, and even this is only nominally true, because the assumed C and O abundances are quite different. In addition, the assumed mass-loss histories are completely different: the Torino models assume mass loss as prescribed by Reimers (1975), whereas the Monash models use the prescription by Vassiliadis & Wood (1993, 1994) based on the period/mass-loss relation for LMC stars. Still, the general trends of the relevant quantities (dredge-up mass, temperature, and the like), with core mass, envelope mass, and metallicity are, generally, similar in the two sets of models. Lugaro et al. (2003b) presented a detailed comparison of the two models for a 3 $M_\odot$ star of solar metallicity. Another difference is that the Torino models assume for the solar C and O abundances the values reported by Allende Prieto et al. (2001, 2002), whereas the Monash models assume the values given by Anders & Grevesse (1989). The new abundances are substantially lower (by factors of 1.5 and 1.9, respectively) and make it easier for a star to become a carbon star. Indeed, the Monash model for a 2.5 $M_\odot$ star of solar metallicity fails to achieve C > O (Table 4), while the Torino model produces a carbon star for 1.5 $M_\odot$ (except for the $\eta = 0.5$ case) and 2 $M_\odot$ (Table 1). Even for the 3 $M_\odot$ star of solar metallicity, the number of TDUs with C > O in the Torino model is much higher (12) than in the Monash model (4). Part of this discrepancy might be due to the different assumed O abundance, but part of it is probably the result of the fact that in general, the Torino models produce more TDU episodes than the Monash models do (see Tables 1 and 4). The latter do not obtain any TDU for stars of $M \leq 2.25\ M_\odot$ and solar metallicity. As far as the Si isotopic shifts are concerned, these are much smaller for the low-mass (1.75 and 1.9 $M_\odot$) Monash models, comparable to the 1.5 $M_\odot$, $\eta = 0.5$ case of the Torino model. However, for $M = 3\ M_\odot$, the shifts are similar (Tables 1 and 4 and Figs. 6*g* and 8*d*), and for $M = 5\ M_\odot$, they are somewhat larger for the Monash model (Figs. 6*h* and 8*f*). One significant difference between the models is that the 4 $M_\odot$ (for $Z = 0.004$) and 5 $M_\odot$ Monash models experience HBB, leading to low $^{12}C/^{13}C$ ratios, and for solar metallicity do not allow the stars to become carbon stars (Table 4). In contrast, no HBB is seen in the 5 $M_\odot$ Torino models, which produce high final $^{12}C/^{13}C$ and C/O ratios (Table 1). HBB is found in FRANEC models of solar metallicity and $M \geq 6\ M_\odot$.

## 4. COMPARISON OF SiC DATA WITH THEORETICAL MODELS

The C and Si isotopic ratios of mainstream, Y, and Z grains are plotted and compared with theoretical predictions in Figures 9, 10, 12, and 13. In Figures 9 and 10 we plot the isotopic ratios measured in the grains as $^{12}C/^{13}C$ ratios and $\delta^{29}Si$ and $\delta^{30}Si$ values (the latter as in Fig. 2) and compare them with predictions (Figs. 6 and 8). However, for a comparison it is more meaningful to separate the GCE effect from the effect of nucleosynthesis. Thus, for Figures 12 and 13 we decomposed the measured Si isotopic ratios into two components, one expressing the GCE of the Si isotopes, and the other, the effect of nucleosynthesis in the parent stars of the grains. The two parameters defined to denote these components are $\delta^{29}Si_{init}$ and $\Delta^{30}Si$ (Fig. 11). The first is the initial $^{29}Si/^{28}Si$ ratio (expressed as a $\delta$-value) of a grain's parent star, and the second is the isotopic shift of the $^{30}Si/^{28}Si$ ratio due to stellar nucleosynthesis. To obtain these two parameters we project a given grain composition along a line representing the results of TDU in AGB stars obtained from the nucleosynthesis models onto the assumed Galactic evolution line (Fig. 11). Since, strictly speaking, we do not know exactly where this line plots, we chose two possible GCE lines. In agreement with the assumption made by the theoretical models, we assume that this line has a slope of 1 on a $\delta$-value three-isotope plot and goes through the solar composition ($\delta^{29}Si = \delta^{30}Si = 0$). The second assumption is that the GCE line is represented by a best-fit line through the Si isotopic compositions of the mainstream grains (this case is shown in Fig. 11). For each of these two cases we projected the grain compositions along average slopes representing the predictions of the models with the Bao et al. (2000) and the Guber et al. (2003) neutron-capture cross sections to obtain the plots shown in Figures 12 and 13. In Figure 12, we also plot the final shifts $\Delta^{30}Si$ predicted by models with different masses and metallicities, the latter as expressed by the different assumed initial $\delta^{29}Si_{init}$ values.

As can be seen in Figure 9, the theoretical models can account only for the isotopic compositions of some of the mainstream grains and of some Y grains. There are two key discrepancies between grain data and models, one associated with the Si isotopic ratios and the other with the C isotopic ratios. The problem with the Si isotopic ratios is that most of the mainstream grains (and Y grains) have $^{29}Si/^{28}Si$ and $^{30}Si/^{28}Si$ ratios higher than the solar ratios, although the grains are older than the solar system. However, the models starting with the highest Si isotopic ratios, those for solar metallicity starting with solar isotopic ratios, cannot reproduce the compositions of mainstream grains and Y grains with higher than solar Si isotopic ratios. This is most clearly seen in Figure 12, where $\delta^{29}Si_{init}$ values range up to 200‰, whereas the models with solar metallicity have $\delta^{29}Si_{init} = 0$ and models with lower than solar metallicity have $\delta^{29}Si_{init} < 0$. This problem has been discussed at length by various authors (Brown & Clayton 1992; Gallino et al. 1994; Timmes & Clayton 1996; Clayton & Timmes 1997; Alexander & Nittler 1999; Lugaro et al. 1999; Clayton 2003). To take this problem into account in the theoretical models, we could either extend them to higher than solar metallicities or we could replace each Si isotopic ratio in the models with a distribution ranging to higher ratios, the way it is schematically expressed by the ellipses shown in Figure 3. If this is done, the low-mass models can successfully explain the C and Si isotopic ratios of the mainstream grains. The problem with the C isotopic ratios in Y and especially in Z grains is that in all models the $^{12}C/^{13}C$ and C/O ratios increase substantially before there is any noticeable change in the Si isotopic ratios. This is clearly seen in Figure 9, but also in Figures 6 and 8, where for almost all models C = O is reached while the Si isotopic ratios in the envelope are still close to the initial ones (see also Tables 1 and 4). If we go to lower than solar metallicity values, which is necessary to produce the large Si isotopic shifts seen in Z grains and in some Y grains, the $^{12}C/^{13}C$ ratios predicted by the models become much higher than the ratios measured in those grains (see Figs. 9 and 13). The reason is that the increased TDU efficiency in low-metallicity stars that produces the required $^{30}Si$ excesses also mixes large amounts of $^{12}C$ into the envelope, resulting in large $^{12}C/^{13}C$ ratios. We return to this problem below.

Inspection of Figure 10 shows that except for the already mentioned problem of the high Si isotopic ratios of the mainstream and some Y grains, the Si isotopic compositions of most other grains can be reproduced by some of the models. In order to achieve the large isotopic shifts in $^{30}Si$ shown by some Z grains, a mass of 3 $M_\odot$ and low metallicity ($Z = 0.003$ for the Torino models and $Z = 0.004$ for the Monash model) are required. However, the Z grains with small $^{29}Si/^{28}Si$ ratios are covered only by the models that use the Guber et al. (2003) cross sections. The Torino models with the Bao et al. (2000) cross sections

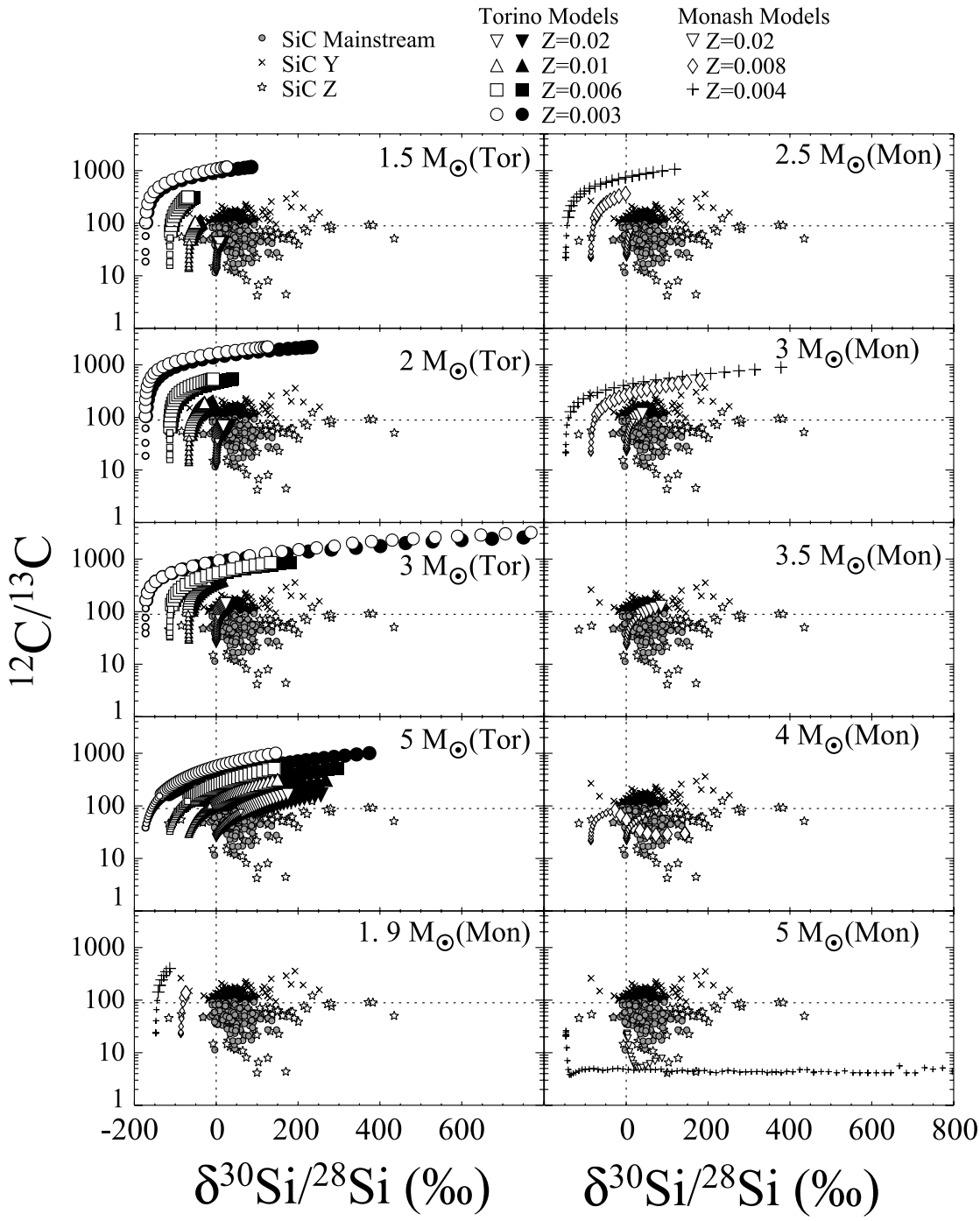


FIG. 9.—$^{12}C/^{13}C$ and $^{30}Si/^{28}Si$ (expressed as $\delta$-values) ratios of mainstream, Y, and Z SiC grains compared with the theoretical predictions of the Torino and Monash models for different masses and metallicities. For the Torino mass 1.5 and 2 $M_{\odot}$ models we plotted the $\eta = 0.3$ case. In the Torino models the open symbols indicate the Bao et al. (2000) neutron-capture cross sections for the Si isotopes, and the filled symbols indicate the Guber et al. (2003) cross sections. Small symbols indicate C < O, and large symbols, C > O. As can be seen, in almost all models the $^{12}C/^{13}C$ ratios increase rapidly before any shifts in the Si isotopic ratios occur. In the models that produce large enough Si isotopic shifts to account for the grain data, the corresponding C isotopic ratios are much too high. Exceptions are the Monash mass 4 and 5 $M_{\odot}$ models, which show the effect of hot bottom burning, which lowers the $^{12}C/^{13}C$ ratio.

and the Monash models, which also use these cross sections, miss these grains completely (Fig. 10). This is best seen in the top and bottom panels of Figure 12. For both assumptions of the GCE line, Z grains projected back along evolution lines based on the Bao et al. (2000) cross sections give $\delta^{29}Si_{init}$ values that are much lower than the initial values covered by the assumed metallicities. In order to obtain such low initial values, one would have to go to much lower metallicities. However, lower metallicities than those in the models are expected to result in even larger shifts in $^{30}Si$ than the extrapolated values. Thus, the Si isotopic ratios of the grains clearly favor the Guber et al. (2003) neutron-capture cross sections. From Figures 10 and 12 we conclude that models with the Guber et al. (2003) cross sections and masses between 2 and 3 $M_{\odot}$ cover the grain data reasonably well if we incorporate a range of $\delta^{29}Si_{init}$ values, if the assumed relationship between $\delta^{29}Si_{init}$ and metallicity is correct, and if the grains only form after cessation of TDU; otherwise, we would see grains between 0 and the model values (cf. Fig. 16 and associated discussion in Nittler & Alexander 2003). The Torino 5 $M_{\odot}$ model predicts $\Delta^{30}Si$ values higher than those found in most of the

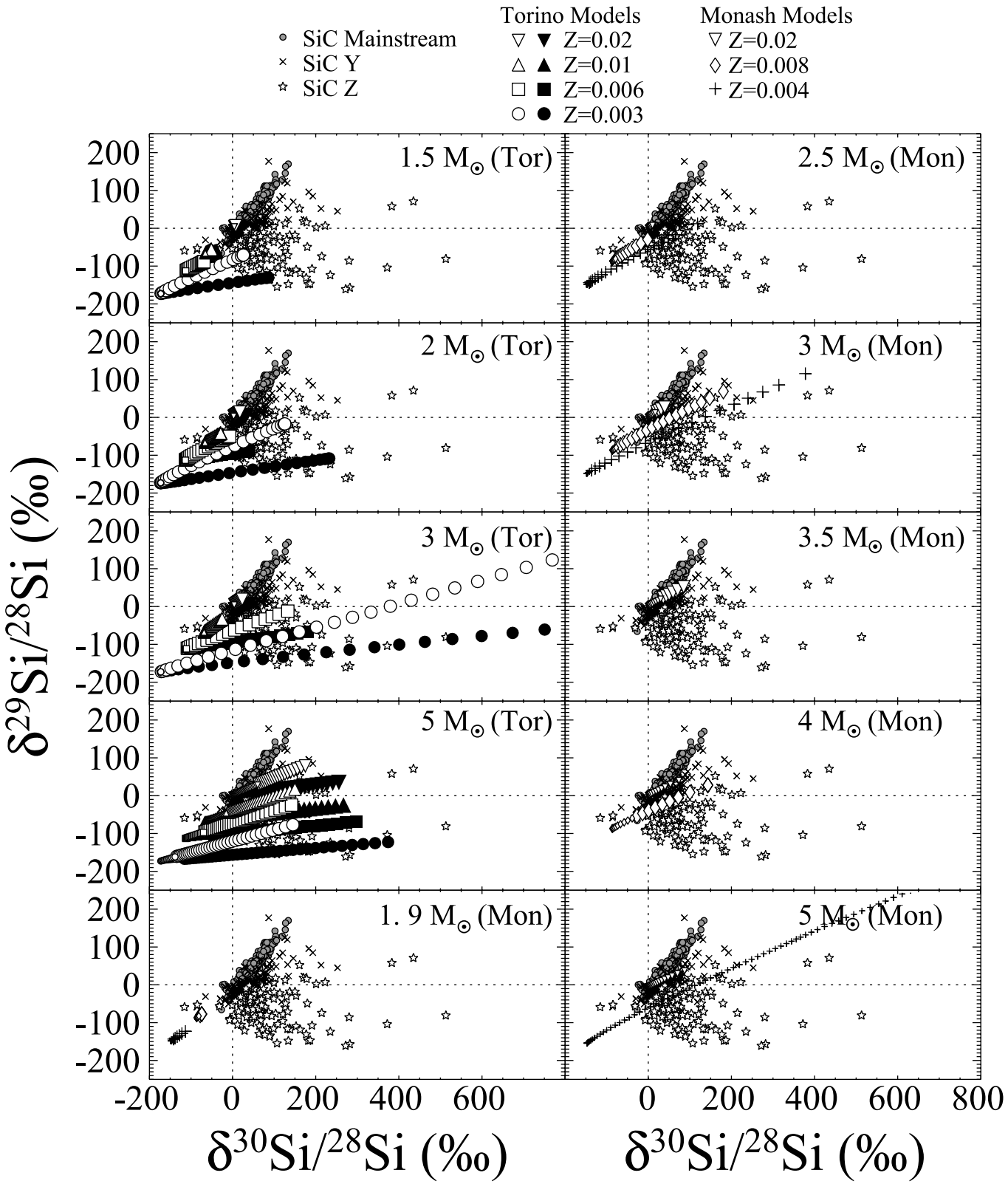


FIG. 10.—Silicon isotopic ratios (expressed as $\delta$-values) of mainstream, Y, and Z SiC grains compared with the theoretical predictions of the Torino and Monash models for different masses and metallicities. As in Fig. 9, for the Torino mass 1.5 and 2 $M_{\odot}$ models we plotted the $\eta = 0.3$ case. In the Torino models the open symbols indicate the Bao et al. (2000) cross sections, and the filled symbols, the Guber et al. (2003) cross sections for the Si isotopes. Small symbols indicate C $<$ O, and large symbols, C $>$ O. According to these plots, only the models based on the Guber et al. (2003) cross sections cover the grain data for the assumed metallicities. To achieve this with the Bao et al. (2000) cross sections (which are also used in the Monash models), one would have to go to much lower metallicities.

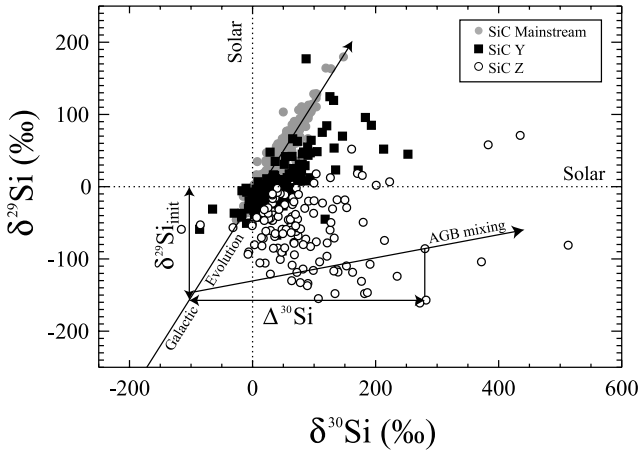


FIG. 11.—Schematic picture of the deconvolution of the Si isotopic ratios of mainstream, Y, and Z grains into two new parameters, $\delta^{29}Si_{init}$ and $\Delta^{30}Si$. Here $\delta^{29}Si_{init}$ is the initial $\delta^{29}Si/^{28}Si$ value of the parent star before any changes in the Si isotopic ratios due to nucleosynthesis had occurred, and $\Delta^{30}Si$ is the change in the $\delta^{30}Si/^{28}Si$ value due to the TDU in AGB stars. The Si isotopic composition of a given grain is projected along the Si isotopic evolution line in the AGB stars (see Figs. 6 and 8) onto the Galactic evolution line. In this figure the Galactic evolution is assumed to proceed along the best-fit line through the mainstream grains.

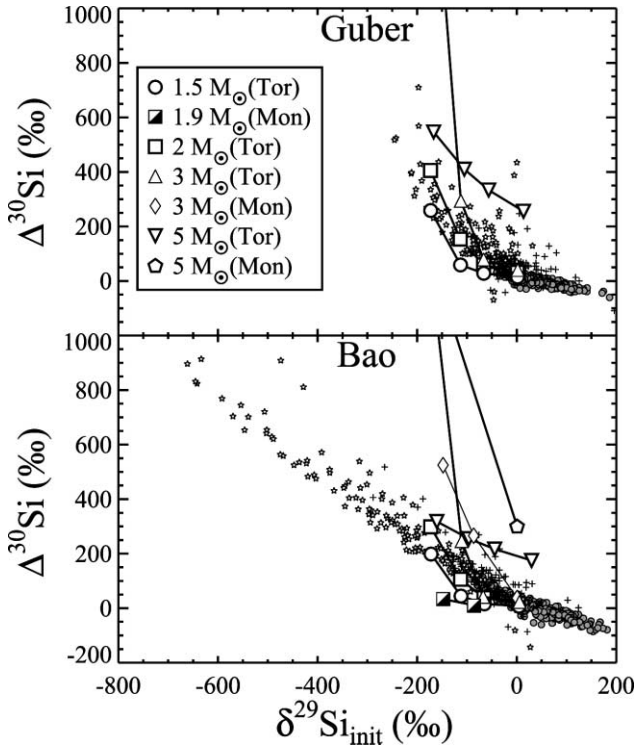


FIG. 12.—Inferred isotopic shifts $\Delta^{30}Si$ plotted against $\delta^{29}Si_{init}$ of the parent stars for mainstream, Y, and Z presolar SiC grains. The symbols for the different grain types are the same as those in Figs. 9 and 10. For the definition of $\Delta^{30}Si$ and $\delta^{29}Si_{init}$, see Fig. 11. The Si isotopic compositions are projected along lines corresponding to the Guber et al. (2003) models and Bao et al. (2000) models (see Figs. 6 and 8) onto a slope = 1 Galactic evolution line. Also plotted are the maximal isotopic shifts in $\Delta^{30}Si$ predicted by AGB models for different masses and metallicities. Model data points for a given mass but varying metallicity are connected by lines. This way of plotting the grain data shows even more impressively than the plots in Fig. 10 that the Guber et al. (2003) cross sections can account for the grain data much better than the Bao et al. (2000) cross sections.

other models and can also explain the ratios measured in Z grains. However, the isotopic compositions of Mo and Zr in mainstream grains are best explained by low-mass parent stars (Lugaro et al. 2003a), and it is quite possible that the Y and Z grains also originated from such stars. The main argument against an intermediate-mass origin of the Y and Z grains is that these stars suffer from HBB that prevents them from becoming C-rich and thus prevents the formation of SiC. This is even more true at low metallicities. This is clearly shown for the Monash 5 $M_\odot$ model.

Let us return to the problem of the C isotopic ratios. As already stated and as seen in Figures 9 and 13, the $^{12}C/^{13}C$ ratios predicted for the low-metallicity cases that produce large enough Si isotopic shifts are much higher than the ratios found in the grains. Exceptions are the Monash 4 $M_\odot$ ($Z = 0.008$) and 5 $M_\odot$ ($Z = 0.02$ and 0.004) models. In the 4 $M_\odot$ model the $^{12}C/^{13}C$ ratio first rises from its initial value of 20 to ~80 but then decreases to 28. In the 5 $M_\odot$ models the $^{12}C/^{13}C$ ratios hardly rise at all above the initial values and drop to final values between 8 and 16 (Table 4) because of HBB. Proton captures in the CNO cycle turn $^{12}C$ into $^{13}C$, reducing the $^{12}C/^{13}C$ ratio, but also convert most of the CNO elements into $^{14}N$, so that in the $Z = 0.02$ models for these two masses the envelope does not achieve C > O (see Table 4). The Monash 4 $M_\odot$, $Z = 0.008$ model can produce C and Si isotopic ratios that overlap with those of some Z grains; however, as already mentioned, we doubt that Y and Z grains come from intermediate-mass stars.

Another process that circulates envelope material to regions in giant stars hot enough to expose it to proton-capture reactions is called cool bottom processing (CBP). This extra mixing process, postulated to occur in low-mass ($\leq$1.65 $M_\odot$) stars on the red giant branch (RGB) and AGB, was originally proposed in order to explain the low $^{12}C/^{13}C$ ratios in RGB stars and the $^{18}O$ depletions of Group 2 presolar oxide grains (Charbonnel 1995; Wasserburg et al. 1995; Abia & Isern 1997; Boothroyd & Sackmann 1999). Nollet et al. (2003) subsequently extended CBP to TP-AGB stars of higher mass, where it can occur in stars with a 3 $M_\odot$ mass and solar and lower than solar metallicity (Wasserburg et al. 2006), and included the production of $^{26}Al$ in their model. In this process, material is circulated from the convective envelope through the underlying radiative zone to hot regions close to the H-burning shell. Nollet et al. (2003) use two parameters to describe the action of CBP: (1) the rate of mixing as expressed by the amount of circulated material, $dM/dt$, expressed in $M_\odot$ yr$^{-1}$, and (2) the maximum temperature experienced by the circulated material. As is the case for the $^{16}O/^{18}O$ ratio, the $^{12}C/^{13}C$ ratio is mostly affected by the first parameter. CBP on the RGB has previously been invoked to explain the fact that Z grains have lower than solar $^{12}C/^{13}C$ ratios (Hoppe et al. 1997b). However, as discussed by Nittler & Alexander (2003) and illustrated by Figure 13, CBP on the RGB is not sufficient to explain the $^{12}C/^{13}C$ ratios in Z grains. In Figure 13 we plot the C isotopic ratios versus $\Delta^{30}Si$ of SiC grains together with the Torino stellar models with the Guber et al. (2003) cross sections. For the 1.5 and 2 $M_\odot$ mass models we assumed, in addition to the models shown in Figure 9, which assumed initial $^{12}C/^{13}C$ ratios at the beginning of the AGB phase between 12 (for $Z = 0.02$) and 18.5 (for $Z = 0.003$), an initial ratio of 3.5, the equilibrium value for H burning in the CNO cycle. This was done under the extreme assumption that CBP on the RGB had lowered the ratio in the envelope to this value. As can be seen in the figure, even under this extreme assumption, the $^{12}C/^{13}C$ ratios for the two cases with the lowest metallicity are higher than those measured in the Z grains. CBP is needed on the AGB as well in order to achieve the C isotopic ratios of the Z grains.

Figure 14 shows a plot of the SiC data together with five different AGB models for the evolution of the C isotopic ratios. The

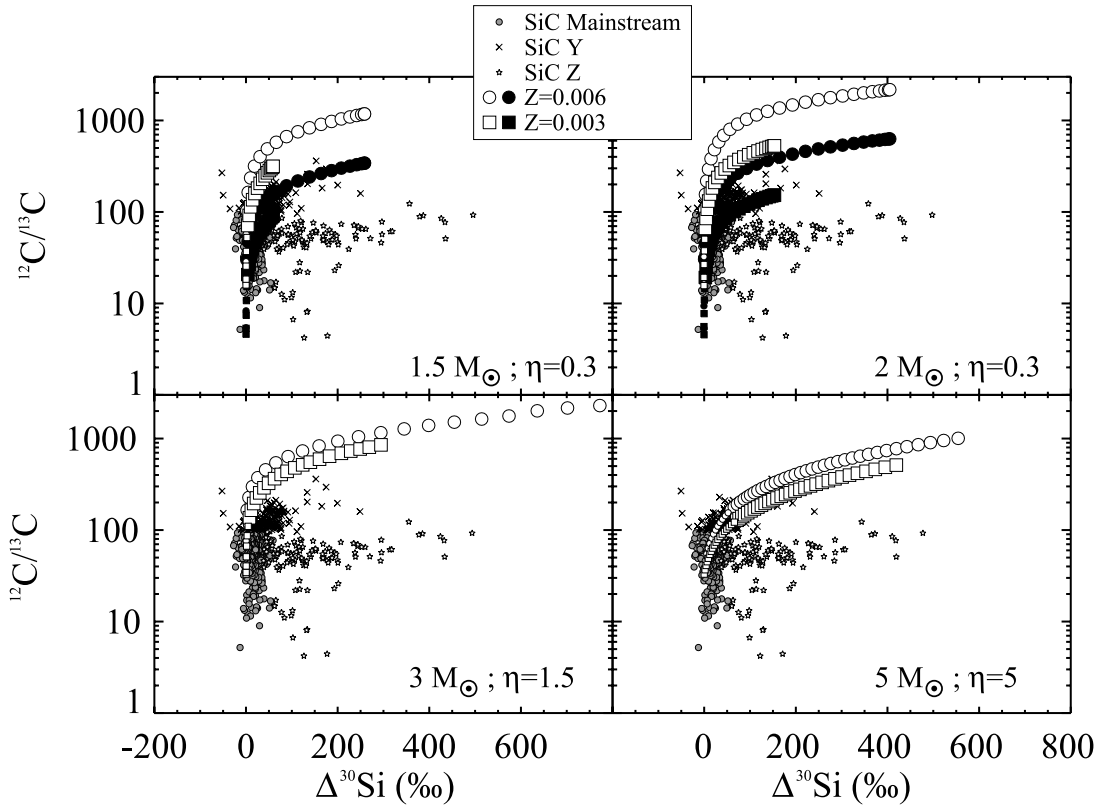


FIG. 13.—Plots of $^{12}C/^{13}C$ ratios against the AGB shifts $\Delta^{30}Si$ for presolar SiC grains from AGB stars. Also plotted are theoretical predictions for the AGB evolution of these isotopic ratios by the Torino models based on the Guber et al. (2003) cross sections for low-metallicity stars with $Z = 0.006$ and $Z = 0.003$. Small symbols indicate $C < O$, and large symbols, $C > O$. As has already been seen from Fig. 9, the predicted $^{12}C/^{13}C$ ratios are much too high to account for the grain data. This is even the case if we assume that for the 1.5 and 2 $M_\odot$ models the initial $^{12}C/^{13}C$ ratio at the beginning of the TP-AGB phase is 5 (*solid symbols*) because of CBP on the red giant branch.

open circles represent the 2 $M_\odot$, $\eta = 0.3$, $Z = 0.003$ model scaled to an initial $^{12}C/^{13}C$ ratio of 5, but with no CBP on the AGB (closely similar to the filled circles in Fig. 13, *top right*). The other curves show the same model adjusted to approximate the effects of CBP on the AGB. The squares indicate one case in which we assume that CBP keeps the $^{12}C/^{13}C$ ratio in the envelope at a constant value of 10 during seven (*open symbols*) and nine (*gray symbols*) pulses (Nollett et al. 2003). Then the CBP is turned off, and TDU again results in increasing $^{12}C/^{13}C$ ratios. In the second case (*triangles*) the CBP during early thermal pulses maintains a lower $^{12}C/^{13}C$ ratio of 3.5. It is clear that by adjusting the initial C isotopic ratio, as well as the circulation rate and duration of CBP during the TP-AGB phase, we can successfully match the grain data. Possible exceptions are a few Z grains with $^{12}C/^{13}C < 10$. HBB in intermediate-mass AGB stars will produce such low ratios (see the 5 $M_\odot$, $Z = 0.004$ Monash model in Fig. 9 or the 4 $M_\odot$, $Z = 0.004$ in Lattanzio & Forestini 1999), but then the shift in $^{30}Si$ is expected to be much larger. Furthermore, such stars usually have $C < O$ (the 5 $M_\odot$ , $Z = 0.004$ Monash model achieves $C > O$ in the envelope only during the last three of 80 TDU episodes). An alternative is that these few grains have a nova (Amari et al. 2001a; Nittler & Hoppe 2004) or supernova (Nittler & Hoppe 2005) origin, but additional isotopic measurements (e.g., of N and Al/Mg) are necessary to confirm these possibilities.

Cool bottom processing is expected to affect also the N isotopic ratios by increasing the $^{14}N/^{15}N$ ratio in the envelope. Unfortunately, fewer Z grains have been analyzed for N isotopes than have been analyzed for C and Si isotopic ratios (compare Figs. 1 and 2). Figure 1 shows that, on average, the $^{14}N/^{15}N$ ratios of Z grains are higher than those of mainstream grains, although lower than expected if the parent stars of the grains experienced CBP and the $^{14}N/^{15}N$ ratio in the envelope approached the CNO equilibrium value. However, N isotopic measurements by ion microprobe can be compromised by contamination with isotopically normal N, be it from foreign objects on the sample mount or from residual gas in the analysis chamber. Such contamination tends to move the measured ratios toward the terrestrial ratio, i.e., toward lower $^{14}N/^{15}N$ ratios, if a grain is depleted in $^{15}N$. The effect is more pronounced for small grains, and Z grains are generally smaller than mainstream grains. This sets an upper limit on the $^{14}N/^{15}N$ ratio that can be measured in small grains. We therefore do not pursue any modeling of the N isotopic ratios during CBP. To make this meaningful would require cleaner N isotopic analyses on Z grains. We can only hope that such analyses will be obtained in the future.

Although CBP is not understood on first principles, apparently not all stars undergo it during their AGB phase (Abia & Isern 1997). Thus, it is puzzling why we do not find SiC grains from low-metallicity carbon stars that have high $^{12}C/^{13}C$ ratios. As discussed above, one process that could limit the maximum $^{12}C/^{13}C$ ratio in SiC grains from AGB stars is CBP. Another possible explanation comes from the fact that in such stars not only the $^{12}C/^{13}C$ ratios but also the C/O ratios are predicted to be very high (see Tables 1 and 4). Under these conditions, graphite and not SiC is expected to condense (Lodders & Amari 2005; Bernatowicz et al. 2006). Thus, the increase in the C/O ratios during TDU in low-metallicity AGB stars could plausibly limit the maximum $^{12}C/^{13}C$ ratio that can be found in SiC grains from such stars, because if the C/O ratio becomes too high, SiC does not condense anymore. We actually seem to have examples of condensates from low-metallicity AGB stars with high $^{12}C/^{13}C$ ratios in the form of presolar graphite grains in meteorites. Amari et al. (1995b)

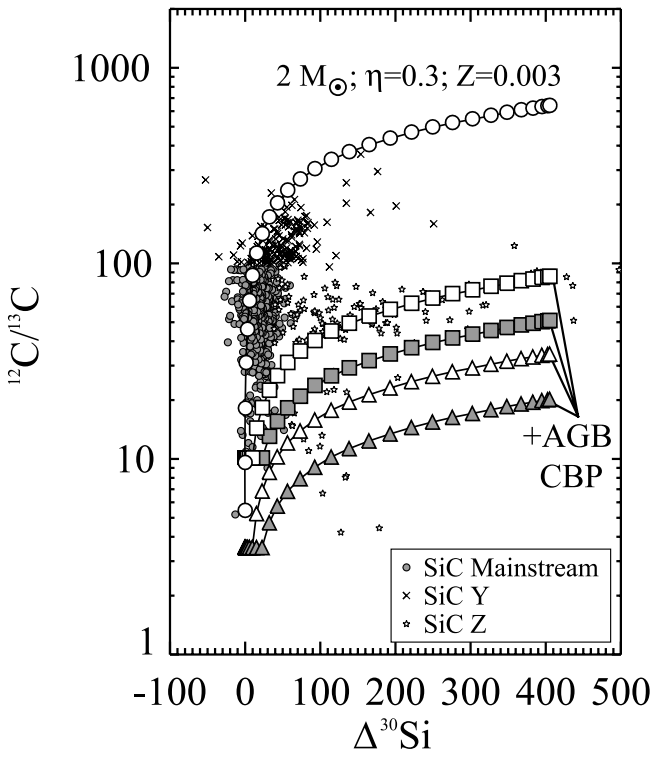


FIG. 14.—Same grain data as in Fig. 13. The open circles denote the original $2\,M_{\odot}, Z = 0.003, \eta = 0.3$ Torino model with an initial $^{12}C/^{13}C$ ratio of 5. The other four models include CBP on the AGB by assuming that CBP acts by keeping the $^{12}C/^{13}C$ ratio in the envelope at a constant value for a certain number of pulses. After these pulses CBP terminates and TDU again results in an increase of the $^{12}C/^{13}C$ ratio for the rest of the TP-AGB phase. *Squares,* AGB CBP $^{12}C/^{13}C$ ratio is 10; *triangles,* the ratio is 3.5; *open symbols,* CBP during seven pulses; *filled symbols,* CBP during nine pulses.

measured noble gases in different density fractions of Murchison graphite grains and found that the Kr isotopic ratios in the highest density fraction, KFC1 (2.15–2.20 g cm$^{-3}$), indicated an AGB origin. The C isotopic ratios in the two highest density fractions of graphite from Murchison show (except for some isotopically normal grains) a bimodal distribution with peaks at ~10 and ~600–700 (Hoppe et al. 1995; Amari et al. 2004). Many grains in these two fractions, KFB1 (2.1–2.15 g cm$^{-3}$) and KFC1, have Si isotopic ratios similar to those of SiC Z grains, namely, large $^{30}$Si excesses (Amari et al. 1995c, 2005). A similar result was recently obtained for high-density graphite grains from the CI carbonaceous chondrite Orgueil (Jadhav et al. 2006). In three fractions comprising the densities 2.02–2.30 g cm$^{-3}$, grains show large $^{30}$Si (and sometimes $^{29}$Si) excesses. These $^{30}$Si excesses are mostly observed in grains with large $^{12}C/^{13}C$ ratios, and the most likely explanation is that these graphite grains originated in low-metallicity AGB stars. There is also recent observational evidence supporting a dominance of graphite over SiC grains in low-metallicity AGB stars. Sloan et al. (2005) reported *Spitzer* observations of carbon stars in the Small Magellanic Cloud and found little evidence of SiC features commonly seen in Galactic C-rich AGB stars.

## 5. GALACTIC EVOLUTION OF THE Si ISOTOPES

The Galactic chemical evolution of the elements leads not only to changes of elemental but also to changes of isotopic abundances throughout the history of the Galaxy. Models of GCE indicate that the $^{29}Si/^{28}Si$ and $^{30}Si/^{28}Si$ ratios increase with Galactic age and thus with increasing metallicity (Timmes & Clayton 1996). The basic tenet of the present paper is that variations in the Si isotopic ratios of different presolar SiC grains indicate an origin in AGB stars of varying metallicities. We compared the Si isotopic ratios of the grains with the predictions of theoretical models for stars with different metallicities. For these models we had to assume a relationship between the parent star's initial isotopic composition and metallicity. However, metallicity not only determines the initial isotopic ratios of the parent stars but also strongly affects changes in the Si isotopic ratios by *n*-capture nucleosynthesis during the TP-AGB phase of the stars. We thus can try to determine the metallicities of the parent stars of individual SiC grains from the Si isotopic shifts (mostly $\Delta^{30}$Si, changes in the $^{30}Si/^{28}Si$ ratio; Fig. 11) and compare the initial inferred $^{29}Si/^{28}Si$ ratios with the metallicities obtained in this way. By this method we can obtain the parent star's initial $^{29}Si/^{28}Si$ ratios as function of metallicity or, in other words, the Galactic evolution of this Si isotopic ratio.

The main problem with this approach is that the Si isotopic shifts also strongly depend on the masses of the parent stars, and without an independent determination of this, we cannot obtain a unique solution. Furthermore, the Si isotopic ratios in the envelope of a given star change throughout the TP-AGB phase as more and more material that experienced neutron capture in the He shell is mixed into the envelope by TDU. Amari et al. (2001b) and Zinner et al. (2001) have obtained a crude estimate of the evolution of the $^{29}Si/^{28}Si$ ratio as a function of metallicity by using averages for these parameters from the mainstream, Y, and Z grains. We can try to improve on this by considering individual grains, but we have to make certain assumptions. First, we assume that all Z grains originated from stars with the same mass but with different metallicities and that the grains formed at the end of the TP-AGB phase when the Si isotopic shifts reached their maximum values. The latter assumption is not absolutely correct, because AGB stars lose mass throughout the TP phase. However, more than half of the C/O > 1 envelope is lost after TDU ceases with an identical isotopic composition during the so-called superwind phase (VW93), and there is recent astronomical evidence that most mass is lost during the superwind phase (van Loon et al. 2005). Molybdenum isotopic ratios in mainstream grains (Lugaro et al. 2003a) also seem to indicate that the grains were formed during late pulses after a large amount of *s*-process material had been mixed into the envelope. With these assumptions we interpolated between the final $\Delta^{30}$Si values from the Torino AGB model for a given mass and Reimers parameter and different metallicities, in order to obtain the metallicity that reproduces the $\Delta^{30}$Si value of each grain.

Plots of the initial $\delta^{29}Si/^{28}Si$ values as functions of the thus determined metallicity obtained for the Z grains are shown in Figure 15 for four different combinations of the mass and Reimers parameter $\eta$ and for the Guber et al. (2003) cross sections. Filled symbols denote the case in which the data points were extrapolated to the mainstream correlation line, and open symbols, the case in which they were extrapolated to the slope = 1 GCE line. The large open circles depict the initial $\delta^{29}Si/^{28}Si$ values assumed in the Torino models, and the broken line represents the GCE of the Si isotopes derived by Timmes & Clayton (1996) and adjusted to go through $\delta^{29}Si/^{28}Si_{init} = 0$ for solar metallicity. One obvious observation is that for all three choices of stellar mass the GCE obtained from the Z grains and the AGB models differs significantly from the Timmes & Clayton (1996) line. The Z grain data indicate that the GCE line reaches higher $^{29}Si/^{28}Si$ ratios at much lower metallicity ($Z \leq 0.01$), but after that the evolutionary slope becomes much shallower. The evolution derived from the grain data is in fairly good agreement with the evolution of the Si isotopes assumed in the Torino and Monash

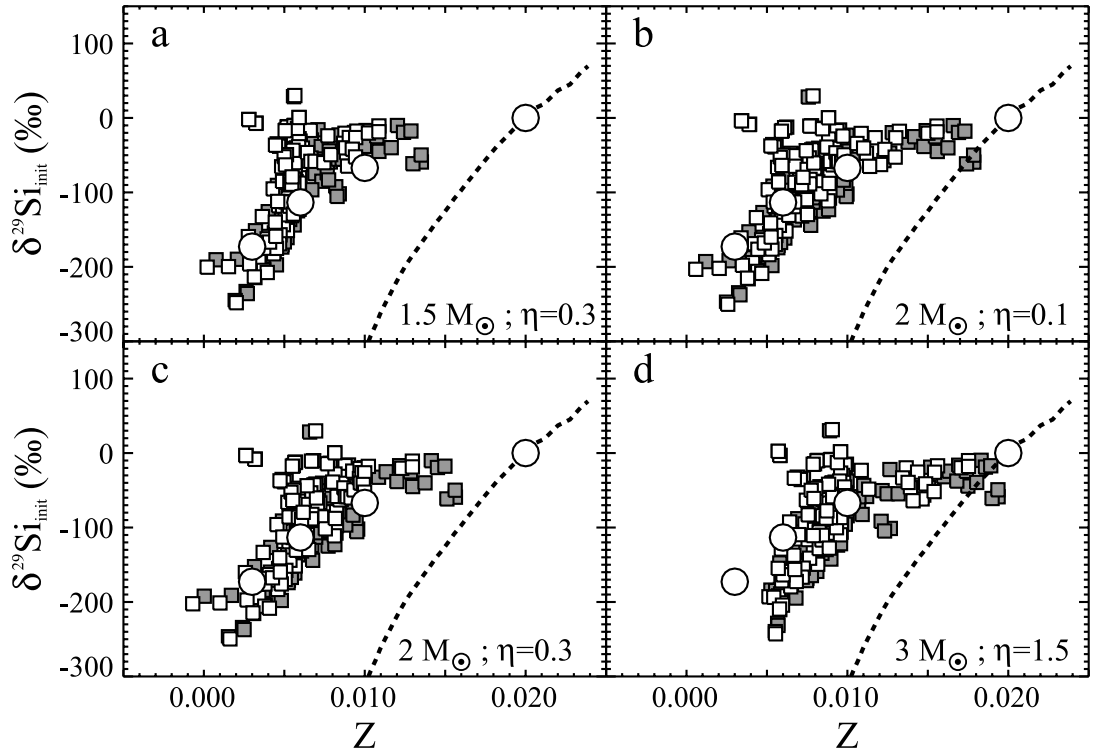


FIG. 15.—For each Z grain the initial $\delta^{29}Si/^{28}Si$ value determined according to Fig. 11 is plotted against the metallicity obtained by interpolating the final $\Delta^{30}Si$ shifts between Torino models of a given mass and Reimers parameter but different metallicities. The results are shown for four different combinations of mass and Reimers parameter. Open symbols depict extrapolation to the slope = 1 evolution line, and filled symbols, extrapolation to the mainstream correlation line (Fig. 11). The large open circles are the initial $\delta^{29}Si/^{28}Si$ values assumed for the Torino models on the basis of enhancements of $^{28}Si$, an $\alpha$ nucleus, over the two other Si isotopes. The broken line shows the GCE model by Timmes & Clayton (1996). All four plots show that the Galactic evolution obtained from the grain data and the AGB models differs significantly from the GCE model.

models. This suggests that the effect from contributions from Type Ia supernovae, which produce essentially pure $^{28}Si$, in the later phases of Galactic evolution (Timmes et al. 1995) is even more important than was assumed in the GCE model by Timmes & Clayton (1996). This conclusion has previously been made by Travaglio et al. (1999) and Woosley et al. (2002). On the other hand, the fast rise in the $^{29}Si/^{28}Si$ (and $^{30}Si/^{28}Si$) at low metallicities as evidenced by the grain data might also indicate higher yields of $^{29}Si$ and $^{30}Si$ in low-metallicity SNe II than models predict. That SN models underproduce $^{29}Si$ relative to $^{30}Si$ compared to the solar ratio is a well-known problem, and various authors (Timmes & Clayton 1996; Lugaro et al. 1999; Alexander & Nittler 1999) adjusted the $^{29}Si/^{30}Si$ ratio to the solar ratios at solar metallicity. The slow rate of increase of the Si isotopic ratios in the Galactic disk at the time of solar system formation and after implied by the grain data is supported by the isotopic composition of present-day Galactic cosmic rays, which are believed to sample the local Galactic environment. Satellite experiments indicate that the Si isotopic ratios are solar within ~10% (Lukasiak et al. 1994; Webber et al. 1997). Much higher ratios are expected if the evolution of the Si isotopes proceeded according to the Timmes & Clayton (1996) model. There are a few SiC grains with $\delta^{29}Si/^{30}Si$ values around 200. The recent findings of a large spread in the metallicity (by a factor of 3) of stars of a given age (Nordström et al. 2004; Andersen et al. 2005) might explain these extreme ratios.

Figure 16 shows a comparison of the Si isotopic evolution based on the Z grains between a 2 $M_\odot$, $\eta = 0.03$ Torino model using the Guber et al. (2003) cross sections and one using the Bao et al. (2000) cross sections. As we have already discussed earlier, AGB nucleosynthesis with the Bao et al. (2000) cross sections implies much lower metallicities and $\delta^{29}Si/^{28}Si_{init}$ values for the parent stars than those obtained with the Guber et al. (2003) cross sections. However, as seen in Figure 16, the evolution derived with the Bao et al. (2000) cross sections is essentially an extension of the one derived with the Guber et al. (2003) cross sections and still completely different from the Timmes & Clayton (1996) GCE line. We therefore do not see how the appropriate choice of any of the parameters used in our models would result in an agreement of the grain-derived GCE curve with the Timmes & Clayton (1996) model. In order to achieve

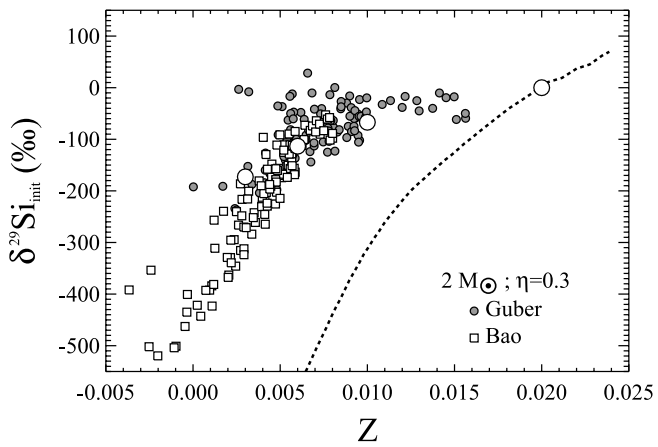


FIG. 16.—Plot of $\delta^{29}Si/^{28}Si$ vs. metallicity, as in Fig. 15, for the 2 $M_\odot$, $\eta = 0.03$ Torino model with extrapolation to the mainstream correlation line for the Guber et al. (2003) and Bao et al. (2000) neutron-capture cross sections of the Si isotopes. The choice of the cross sections strongly affects the metallicities inferred from the grains but does not achieve agreement with the Galactic evolution curve by Timmes & Clayton (1996).

that, the Si predicted isotopic shifts, specifically $\Delta^{30}$Si, would have to be much larger at metallicity values of $Z = 0.01$ and above than the results of both the Torino and Monash models. This is unlikely. The Si isotopic shifts during the TP-AGB phase are almost exclusively determined by capture of neutrons from the $^{22}$Ne neutron source, which is much better understood than the $^{13}$C source, where the strength of the $^{13}$C pocket is essentially a free parameter. This situation is not improved if we relax our assumption that the SiC grains have the Si isotopic ratio reached at the end of the TP-AGB phase. If the SiC grains formed earlier, i.e., with smaller Si isotopic shifts, we do need even lower metallicities of the models to match the Si isotopic data of the grains. This means that the $Z$ data points in the Figure 15 plots will be shifted to the left, and the discrepancy with the GCE models will be worse. We conclude that our way of estimating the Si isotopic ratios for lower than solar metallicities by scaling the $^{29}$Si and $^{30}$Si abundances with the Fe abundance and assuming enhancement of $^{28}$Si (and the other $\alpha$ nuclei) gives a better description of the Galactic evolution of the Si isotopic ratios than the Timmes & Clayton (1996) model. Currently it is not clear why there is such a discrepancy. Above we suggested that low-metallicity SNe II might have higher yields of the heavy Si isotopes than current models predict. Moreover, the Timmes & Clayton (1996) model included the effects of AGB stars, but assumed very different AGB Si isotope yields than have been calculated here. It would be worthwhile to calculate GCE models using the updated AGB yields and to vary the low-metallicity SN II yields to determine how much they have to be increased to match the evolution derived from the SiC grains.

## 6. CONCLUSIONS

We compared the C and Si isotopic ratios of presolar mainstream, Y, and Z SiC grains with the results of theoretical models for nucleosynthesis in TP-AGB stars. We obtained two sets of models (Torino and Monash) for different stellar masses, metallicities, and prescriptions for mass loss and, for the Torino models, two sets of neutron-capture cross sections for the Si isotopes (Bao et al. 2000; Guber et al. 2003). The models give the following results:

1. The increases in the $^{12}$C/$^{13}$C, $^{29}$Si/$^{28}$Si, and $^{30}$Si/$^{28}$Si ratios in the stars' envelopes during TDU are higher for higher stellar mass and lower metallicity.

2. Since $^{22}$Ne is the dominating neutron source affecting the Si isotopes, the Si isotopic shifts hardly depend at all on the strength of the $^{13}$C pocket.

3. In a Si three-isotope diagram the evolution of the Si isotopes proceeds along steeper lines for the Bao et al. (2000) cross sections than for the Guber et al. (2003) cross sections.

The comparison of the model results with grain data leads to the following conclusions:

1. It confirms an AGB star origin for mainstream, Y, and Z SiC grains. These grains must have originated from stars with a range of metallicities, with the metallicity of mainstream grains being higher than that of Y grains, which is in turn higher than that of Z grains.

2. The grains' Si isotopic ratios favor the Guber et al. (2003) cross sections over those of Bao et al. (2000).

3. The $^{12}$C/$^{13}$C ratios predicted for low-metallicity models are much higher than those found in the grains, and cool bottom processing (CBP) must be invoked to explain the C and Si isotopic ratios measured in Z grains.

4. High C/O ratios in low-metallicity stars without CBP might have prevented the formation of SiC grains and led to the condensation of graphite grains instead.

5. Combining Z grain data with the models allows us to infer how the Galactic $^{29}$Si/$^{28}$Si ratio evolves as a function of metallicity. At $Z \leq 0.01$ this ratio rises much faster than predicted by GCE models (Timmes & Clayton 1996).

6. The grain data suggest a low-metallicity source of $^{29}$Si and $^{30}$Si not considered by present GCE models.

We appreciate the detailed review of Achim Weiss that helped in improving this paper. R. G. thanks the Aspen Center for Physics for insightful discussions related to this work during the "Summer School on the *s*-process" organized by R. Reifarth and F. Herwig. This work was supported by NASA grants NNG05GF81G (E. Z.) and NNG04GF61G (L. N.), the Italian MIUR-FIRB project (R. G.), NOW through a VENI grant (M. L.), the Victorian and Australian Partnership for Advanced Computing (A. K.), PRIN MIUR 2004 (O. S.), and the Australian Research Council (J. L.).

## REFERENCES

Abia, C., & Isern, J. 1997, MNRAS, 289, L11
Alexander, C. M. O'D. 1993, Geochim. Cosmochim. Acta, 57, 2869
Alexander, C. M. O'D., & Nittler, L. R. 1999, ApJ, 519, 222
Allende Prieto, C., Lambert, D. L., & Asplund, M. 2001, ApJ, 556, L63
———. 2002, ApJ, 573, L137
Amari, S., Anders, E., Virag, A., & Zinner, E. 1990, Nature, 345, 238
Amari, S., Gao, X., Nittler, L. R., Zinner, E., José, J., Hernanz, M., & Lewis, R. S. 2001a, ApJ, 551, 1065
Amari, S., Hoppe, P., Zinner, E., & Lewis, R. S. 1995a, Meteoritics, 30, 679
Amari, S., Jennings, C., Nguyen, A., Stadermann, F. J., Zinner, E., & Lewis, R. S. 2002, Lunar Planet. Sci. Conf., 33, 1205
Amari, S., Lewis, R. S., & Anders, E. 1994, Geochim. Cosmochim. Acta, 58, 459
———. 1995b, Geochim. Cosmochim. Acta, 59, 1411
Amari, S., Nittler, L. R., Zinner, E., Gallino, R., Lugaro, M., & Lewis, R. S. 2001b, ApJ, 546, 248
Amari, S., Nittler, L. R., Zinner, E., Lodders, K., & Lewis, R. S. 2001c, ApJ, 559, 463
Amari, S., Zinner, E., Gallino, R., & Lewis, R. 2003, Meteoritics Planet. Sci., 38, A66
Amari, S., Zinner, E., & Lewis, R. S. 1995c, in AIP Conf. Proc. 327, Nuclei in the Cosmos III, ed. M. Busso, R. Gallino, & C. M. Raiteri (New York: AIP), 581
———. 2004, Meteoritics Planet. Sci., 39, A13
———. 2005, Meteoritics Planet. Sci., 40, A15
Anders, E., & Grevesse, N. 1989, Geochim. Cosmochim. Acta, 53, 197
Andersen, J., Nordström, B., & Mayor, M. 2005, in ASP Conf. Ser. 336, Cosmic Abundances as Records of Stellar Evolution and Nucleosynthesis, ed. T. G. Barnes III & F. N. Bash (San Francisco: ASP), 305
Angulo, C., et al. 1999, Nucl. Phys. A, 656, 3
Asplund, M. 2005, ARA&A, 43, 481
Asplund, M., Lambert, D. L., Kipper, T., Pollacco, D., & Shetrone, M. D. 1999, A&A, 343, 507
Bao, Z. Y., Beer, H., Käppeler, F., Voss, F., Wisshak, K., & Rauscher, T. 2000, At. Data Nucl. Data Tables, 76, 70
Beer, H., Voss, F., & Winters, R. R. 1992, ApJS, 80, 403
Bernatowicz, T., Fraundorf, G., Tang, M., Anders, E., Wopenka, B., Zinner, E., & Fraundorf, P. 1987, Nature, 330, 728
Bernatowicz, T. J., Amari, S., Zinner, E. K., & Lewis, R. S. 1991, ApJ, 373, L73
Bernatowicz, T. J., Cowsik, R., Gibbons, P. C., Lodders, K., Fegley, B., Jr., Amari, S., & Lewis, R. S. 1996, ApJ, 472, 760
Bernatowicz, T. J., Croat, T. K., & Daulton, T. L. 2006, in Meteorites and the Early Solar System II, ed. D. S. Lauretta & H. Y. McSween, Jr. (Tucson: Univ. Arizona Press), 109
Bernatowicz, T. J., & Zinner, E., eds. 1997, Astrophysical Implications of the Laboratory Study of Presolar Materials (New York: AIP)
Besmehn, A., & Hoppe, P. 2003, Geochim. Cosmochim. Acta, 67, 4693

Boldeman, J. W., Allen, B. J., Musgrove, A. R. de L., & Macklin, R. L. 1975, Nucl. Phys. A, 252, 62
Boothroyd, A. I., & Sackmann, I.-J. 1988a, ApJ, 328, 653
———. 1988b, ApJ, 328, 671
———. 1999, ApJ, 510, 232
Brown, L. E., & Clayton, D. D. 1992, ApJ, 392, L79
Busso, M., Gallino, R., & Wasserburg, G. J. 1999, ARA&A, 37, 239
Cannon, R. C. 1993, MNRAS, 263, 817
Charbonnel, C. 1995, ApJ, 453, L41
Choi, B.-G., Wasserburg, G. J., & Huss, G. R. 1999, ApJ, 522, L133
Clayton, D. D. 1997, ApJ, 484, L67
———. 2003, ApJ, 598, 313
Clayton, D. D., & Nittler, L. R. 2004, ARA&A, 42, 39
Clayton, D. D., Obradovic, M., Guha, S., & Brown, L. E. 1991, Lunar Planet. Sci. Conf., 22, 221
Clayton, D. D., & Timmes, F. X. 1997, ApJ, 483, 220
Croat, T. K., Bernatowicz, T., Amari, S., Messenger, S., & Stadermann, F. J. 2003, Geochim. Cosmochim. Acta, 67, 4705
Croat, T. K., Stadermann, F. J., & Bernatowicz, T. J. 2005, ApJ, 631, 976
Denissenkov, P. A., & Tout, C. A. 2003, MNRAS, 340, 722
Denker, A., et al. 1995, in AIP Conf. Proc. 327, Nuclei in the Cosmos III, ed. M. Busso, R. Gallino, & C. M. Raiteri (New York: AIP), 255
Edvardsson, B., Anderson, J., Gustaffson, B., Lambert, D. L., Nissen, P. E., & Tomkin, J. 1993, A&A, 275, 101
El Eid, M. 1994, A&A, 285, 915
Frost, C. A., Cannon, R. C., Lattanzio, J. C., Wood, P. R., & Forestini, M. 1998, A&A, 332, L17
Frost, C. A., & Lattanzio, J. C. 1996, ApJ, 473, 383
Gallino, R., Arlandini, C., Busso, M., Lugaro, M., Travaglio, C., Straniero, O., Chieffi, A., & Limongi, M. 1998, ApJ, 497, 388
Gallino, R., Busso, M., & Lugaro, M. 1997, in Astrophysical Implications of the Laboratory Study of Presolar Materials, ed. T. J. Bernatowicz & E. Zinner (New York: AIP), 115
Gallino, R., Raiteri, C. M., Busso, M., & Matteucci, F. 1994, ApJ, 430, 858
Goriely, S., & Mowlavi, N. 2000, A&A, 362, 599
Guber, K. H., Koehler, P. E., Derrien, H., Valentine, T. E., Leal, L. C., Sayer, R. O., & Rauscher, T. 2003, Phys. Rev. C, 67, 062802
Herwig, F. 2000, A&A, 360, 952
Herwig, F., & Austin, S. M. 2004, ApJ, 613, L73
Herwig, F., Langer, N., & Lugaro, M. 2003, ApJ, 593, 1056
Hoppe, P., Amari, S., Zinner, E., Ireland, T., & Lewis, R. S. 1994, ApJ, 430, 870
Hoppe, P., Amari, S., Zinner, E., & Lewis, R. S. 1995, Geochim. Cosmochim. Acta, 59, 4029
Hoppe, P., Annen, P., Strebel, R., Eberhardt, P., Amari, S., & Lewis, R. S. 1997a, Lunar Planet. Sci. Conf., 28, 599
Hoppe, P., Annen, P., Strebel, R., Eberhardt, P., Gallino, R., Lugaro, M., Amari, S., & Lewis, R. S. 1997b, ApJ, 487, L101
Hoppe, P., & Besmehn, A. 2002, ApJ, 576, L69
Hoppe, P., & Ott, U. 1997, in Astrophysical Implications of the Laboratory Study of Presolar Materials, ed. T. J. Bernatowicz & E. Zinner (New York: AIP), 27
Hoppe, P., Strebel, R., Eberhardt, P., Amari, S., & Lewis, R. S. 1996a, Geochim. Cosmochim. Acta, 60, 883
———. 1996b, Science, 272, 1314
———. 2000, Meteoritics Planet. Sci., 35, 1157
Hoppe, P., & Zinner, E. 2000, J. Geophys. Res., 105, 10371
Huss, G. R., Fahey, A. J., Gallino, R., & Wasserburg, G. J. 1994, ApJ, 430, L81
Huss, G. R., Hutcheon, I. D., & Wasserburg, G. J. 1997, Geochim. Cosmochim. Acta, 61, 5117
Huss, G. R., & Lewis, R. S. 1995, Geochim. Cosmochim. Acta, 59, 115
Hutcheon, I. D., Huss, G. R., Fahey, A. J., & Wasserburg, G. J. 1994, ApJ, 425, L97
Jadhav, M., Amari, S., Zinner, E., & Maruoka, T. 2006, NewA Rev., in press
Käppeler, F., et al. 1994, ApJ, 437, 396
Karakas, A. I. 2003, Ph.D. thesis, Monash Univ.
Karakas, A. I., Lattanzio, J. C., & Pols, O. R. 2002, Publ. Astron. Soc. Australia, 19, 515
Karakas, A. I., Lugaro, M. A., Wiescher, M., Goerres, J., & Ugalde, C. 2006, ApJ, 643, 471
Lattanzio, J., & Forestini, M. 1999, in IAU Symp. 191, Asymptotic Giant Branch Stars, ed. T. Le Bertre, A. Lèbre, & C. Waelkens (San Francisco: ASP), 31
Lattanzio, J., Forestini, M., & Charbonnel, C. 2000, Mem. Soc. Astron. Italiana, 71, 737
Lattanzio, J., Frost, C., Cannon, R., & Wood, P. 1996, Mem. Soc. Astron. Italiana, 67, 729
Lattanzio, J. C. 1986, ApJ, 311, 708
Lattanzio, J. C., Frost, C. A., Cannon, R. C., & Wood, P. R. 1997, Nucl. Phys. A, 621, 435
Lewis, R. S., Tang, M., Wacker, J. F., Anders, E., & Steel, E. 1987, Nature, 326, 160
Lin, Y., Amari, S., & Pravdivtseva, O. 2002, ApJ, 575, 257
Lodders, K., & Amari, S. 2005, Chem. Erde, 65, 93
Lugaro, M., Davis, A. M., Gallino, R., Pellin, M. J., Straniero, O., & Käppeler, F. 2003a, ApJ, 593, 486
Lugaro, M., Herwig, F., Lattanzio, J. C., Gallino, R., & Straniero, O. 2003b, ApJ, 586, 1305
Lugaro, M., Ugalde, C., Karakas, A. I., Görres, J., Wiescher, M., Lattanzio, J. C., & Cannon, R. C. 2004, ApJ, 615, 934
Lugaro, M., Zinner, E., Gallino, R., & Amari, S. 1999, ApJ, 527, 369
Lukasiak, A., Ferrando, P., McDonald, F. B., & Webber, W. R. 1994, ApJ, 426, 366
McWilliam, A. 1997, ARA&A, 35, 503
Messenger, S., Keller, L. P., Stadermann, F. J., Walker, R. M., & Zinner, E. 2003, Science, 300, 105
Mostefaoui, S., & Hoppe, P. 2004, ApJ, 613, L149
Mowlavi, N. 1999, A&A, 344, 617
Nagashima, K., Krot, A. N., & Yurimoto, H. 2004, Nature, 428, 921
Newton, J., Bischoff, A., Arden, J. W., Franchi, I. A., Geiger, T., & Pillinger, C. T. 1995, Meteoritics, 30, 47
Nguyen, A. N., & Zinner, E. 2004, Science, 303, 1496
Nicolussi, G. K., Davis, A. M., Pellin, M. J., Lewis, R. S., Clayton, R. N., & Amari, S. 1997, Science, 277, 1281
Nicolussi, G. K., Pellin, M. J., Lewis, R. S., Davis, A. M., Amari, S., & Clayton, R. N. 1998a, Geochim. Cosmochim. Acta, 62, 1093
Nicolussi, G. K., Pellin, M. J., Lewis, R. S., Davis, A. M., Clayton, R. N., & Amari, S. 1998b, ApJ, 504, 492
Nittler, L. R. 1996, Ph.D. thesis, Washington Univ.
———. 2003, Earth Planet. Sci. Lett., 209, 259
———. 2005, ApJ, 618, 281
Nittler, L. R., & Alexander, C. M. O'D. 2003, Geochim. Cosmochim. Acta, 67, 4961
Nittler, L. R., Alexander, C. M. O'D., Gao, X., Walker, R. M., & Zinner, E. 1997, ApJ, 483, 475
Nittler, L. R., Alexander, C. M. O'D., Gao, X., Walker, R. M., & Zinner, E. K. 1994, Nature, 370, 443
Nittler, L. R., Amari, S., Zinner, E., Woosley, S. E., & Lewis, R. S. 1996, ApJ, 462, L31
Nittler, L. R., & Hoppe, P. 2004, Lunar Planet. Sci. Conf., 35, 1598
———. 2005, ApJ, 631, L89
Nittler, L. R., et al. 1995, ApJ, 453, L25
Nollett, K. M., Busso, M., & Wasserburg, G. J. 2003, ApJ, 582, 1036
Nordström, B., et al. 2004, A&A, 418, 989
Owen, T., Mahaffy, P. R., Niemann, H. B., Atreya, S., & Wong, M. 2001, ApJ, 553, L77
Reddy, B. E., Tomkin, J., Lambert, D. L., & Allende Prieto, C. 2003, MNRAS, 340, 304
Reimers, D. 1975, in Problems in Stellar Atmospheres and Envelopes, ed. B. Baschek, W. H. Kegel, & G. Traving (New York: Springer), 229
Russell, S. S., Ott, U., Alexander, C. M. O'D., Zinner, E. K., Arden, J. W., & Pillinger, C. T. 1997, Meteoritics Planet. Sci., 32, 719
Savina, M. R., Davis, A. M., Tripa, C. E., Pellin, M. J., Gallino, R., Lewis, R. S., & Amari, S. 2004, Science, 303, 649
Schatz, H., Jaag, S., Linker, G., Steininger, R., Käppeler, F., Koehler, P. E., Graff, S. M., & Wiescher, M. 1995, Phys. Rev. C, 51, 379
Schöier, F. L., & Olofsson, H. 2001, A&A, 368, 969
Sloan, G. C., Kraemer, K. E., Matsuura, M., Price, S. D., Wood, P. R., & Egan, M. P. 2005, BAAS Abstr., 206, 06.02
Slodzian, G., Hillion, F., Stadermann, F. J., & Horreard, F. 2003, Appl. Surface Sci., 203–204, 798
Slodzian, G., Hillion, F., Stadermann, F. J., & Zinner, E. 2004, Appl. Surface Sci., 231–232, 874
Straniero, O., Chieffi, A., Limongi, M., Busso, M., Gallino, R., & Arlandini, C. 1997, ApJ, 478, 332
Straniero, O., Domínguez, I., Cristallo, S., & Gallino, R. 2003, Publ. Astron. Soc. Australia, 20, 389
Straniero, O., Gallino, R., & Cristallo, S. 2006, Nucl. Phys. A, in press
Straniero, O., Limongi, M., Chieffi, A., Dominguez, I., Busso, M., & Gallino, R. 2000, Mem. Soc. Astron. Italiana, 71, 719
Tang, M., & Anders, E. 1988, Geochim. Cosmochim. Acta, 52, 1235
Thielemann, F.-K., Arnould, M., & Truran, J. W. 1986, in Advances in Nuclear Astrophysics, ed. E. Vangioni-Flam et al. (Gif-sur-Yvette: Editions Frontières), 525
Timmes, F. X., & Clayton, D. D. 1996, ApJ, 472, 723
Timmes, F. X., Woosley, S. E., & Weaver, T. A. 1995, ApJS, 98, 617

Travaglio, C., Galli, D., Gallino, R., Busso, M., Ferrini, F., & Straniero, O. 1999, ApJ, 521, 691
Vaglio, P., et al. 1998, in Nuclei in the Cosmos V, ed. N. Prantzos & S. Harissopulos (Paris: Editions Frontières), 223
van Loon, J. T., Groenewegen, M. A. T., de Koter, A., Trams, N. R., Waters, L. B. F. M., Zijlstra, A. A., Whitelock, P. A., & Loup, C. 1999, A&A, 351, 559
van Loon, J. T., Marshall, J. R., & Zijlstra, A. A. 2005, A&A, 442, 597
van Loon, J. T., et al. 1998, A&A, 329, 169
Vassiliadis, E., & Wood, P. R. 1993, ApJ, 413, 641 (VW93)
———. 1994, ApJS, 92, 125
Wasserburg, G. J., Boothroyd, A. I., & Sackmann, I.-J. 1995, ApJ, 447, L37
Wasserburg, G. J., Busso, M., Gallino, R., & Nollett, K. M. 2006, Nucl. Phys. A, 777, 5
Webber, W. R., Lukasiak, A., & McDonald, F. B. 1997, ApJ, 476, 766
Whitelock, P. A., Feast, M. W., van Loon, J. T., & Zijlstra, A. A. 2003, MNRAS, 342, 86
Winters, J. M., Le Bertre, T., Jeong, K. S., Nyman, L.-Å., & Epchtein, N. 2003, A&A, 409, 715
Woosley, S. E., Heger, A., & Weaver, T. A. 2002, Rev. Mod. Phys., 74, 1015
Zinner, E. 1998, Annu. Rev. Earth Planet. Sci., 26, 147
———. 2003, in Treatise on Geochemistry, Vol. 1, Meteorites, Planets, and Comets, ed. A. M. Davis, H. D. Holland, & K. K. Turekian (Oxford: Pergamon), 17
Zinner, E., Amari, S., Gallino, R., & Lugaro, M. 2001, Nucl. Phys. A, 688, 102
Zinner, E., Amari, S., Guinness, R., & Jennings, C. 2003, Meteoritics Planet. Sci., 38, A60
Zinner, E., Tang, M., & Anders, E. 1987, Nature, 330, 730
Zinner, E., et al. 2005, Lunar Planet. Sci. Conf., 36, 1691